



Effects of half-sinusoidal nonuniform heating during MHD thermal convection in Cu–Al₂O₃/water hybrid nanofluid saturated with porous media

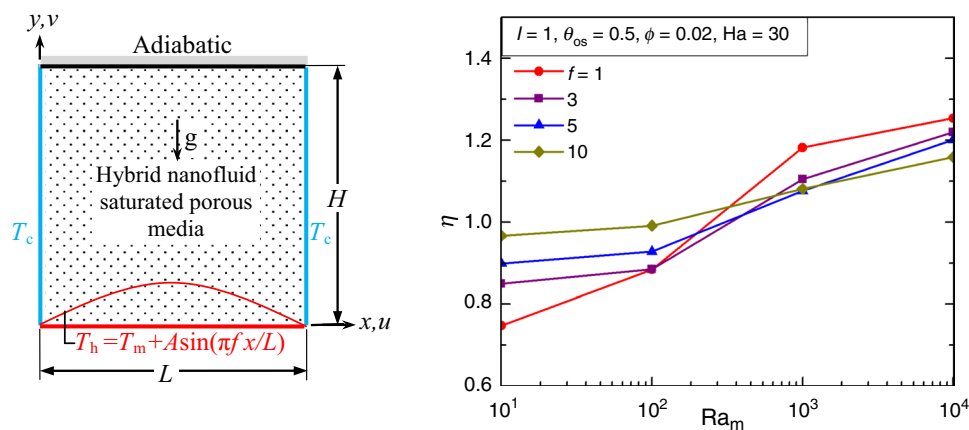
Nirmalendu Biswas¹ · Nirmal K. Manna² · Ali J. Chamkha^{3,4}

Received: 25 March 2020 / Accepted: 22 July 2020 / Published online: 3 August 2020
© Akadémiai Kiadó, Budapest, Hungary 2020

Abstract

The intent of this study is to demonstrate an approach for augmenting heat transfer through porous media subjected to nonuniform heating during the magnetohydrodynamic flow of a hybrid nanofluid of Cu–Al₂O₃/water. The efficacy of such a heating technique is examined utilizing a classical flow geometry consisting of a square cavity. The heating is made at the bottom following a half-sinusoidal function of different frequencies, along with the presence of a uniform magnetic field. The thermal conditions of the cavity, particularly at the bottom wall, drive thermo-hydrodynamics and associated heat transfer. Furthermore, the addition of different types of nanoparticles to the base liquid in order to boost the thermal performance of conventional fluids and mono-nanofluids is a current technique. The coupled nonlinear governing equations are solved numerically in dimensionless forms adapting the finite volume approach, the Brinkman–Forchheimer–Darcy model, local thermal equilibrium and single-phase model. The study is conducted for wide ranges of parametric impacts to analyze global heat transfer performance. The results of this study reveal that the multi-frequency spatial heating during hybrid nanofluid flow can be utilized as a powerful means to improve the thermal performance of a system operating under different ranges of parameters, even with the presence of porous media and magnetic fields. In addition to different heating frequencies, the variations in amplitude (I) and superposed uniform temperature (θ_{os}) to half-sinusoidal heating are also examined thoughtfully in the analysis for different concentrations of Cu–Al₂O₃ nanoparticles. Compared to the base liquid, the hybrid nanofluid can contribute toward higher heat transfer.

Graphic abstract



Keywords Hybrid nanofluid · Porous cavity · Half-sinusoidal heating · Offset temperature · Magnetohydrodynamic (MHD) flow · Natural convection · Heatlines

Extended author information available on the last page of the article

List of symbols

B	Magnetic field (Tesla, $\text{N A}^{-1} \text{m}^{-2}$)
Da	Darcy number
F_c	Forchheimer coefficient
g	Acceleration due to gravity (m s^{-2})
H	Height of the cavity/length scale (m)
Ha	Hartmann number
K	Permeability of porous medium (m^2)
L	Length of the cavity (m)
Nu	Average Nusselt number
P	Dimensionless pressure
Pr	Prandtl number
Ra	Fluid Rayleigh number
Ra_m	Darcy–Rayleigh number
T	Temperature (K)
u, v	Velocity components (m s^{-1})
U, V	Dimensionless velocity components
x, y	Cartesian coordinates (m)
X, Y	Dimensionless coordinates

Greek symbols

α	Thermal diffusivity ($\text{m}^2 \text{s}^{-1}$)
β	Thermal expansion coefficient (K^{-1})
ε	Porosity
η	Heat transfer parameter
θ	Dimensionless temperature
μ	Dynamic viscosity (Ns m^{-2})
ν	Kinematic viscosity ($\text{m}^2 \text{s}^{-1}$)
ρ	Density (kg m^{-3})
σ	Electrical conductivity (μScm^{-1})
ϕ	Volume fraction of nanoparticles
ψ	Dimensionless stream function
Π	Dimensionless heat function

Subscripts

c	Cold
f	Base fluid/liquid
h	Hot
nf	Nanofluid
hnf	Hybrid nanofluid
max	Maximum
os	Offset temperature
s	Solid

Introduction

Proper understanding of buoyancy-driven thermal convection and its control through a porous substrate is an important issue in the perspective of countless industrial as well as domestic applications. Cooling of electronic devices, heat exchangers, chemical reactors, chemical equipment, nuclear waste management, high-efficiency insulators, solar thermal systems, geothermal energy systems, oil and gas production

system, food grain processing (or storage), medical science, biological systems are just a few names in this context. The presence of porous substances (solid matrix with continuous pores) in any process significantly lessens the heat transfer rate of the system; thus, it may need suitable means if heat transfer augmentation or size miniaturization is essentially required. On the other side, buoyancy-driven convection (or natural convection due to temperature gradient) could be a primary choice of cooling means to certain types of appliances due to its simplicity, ease of operation and free from any electromechanical arrangement. Researchers are continually paying their attention to explore the best technique of cooling management for the components/systems of any devices from the past decades to the present time [1–5]. A detailed review on enhanced cooling management in a confined space is reported in Ref. [6, 7].

As a part of remarkable technological advancement, components and devices are getting miniaturized and simultaneously targeting demand for higher efficacy. Thus, components or devices are facing tremendous heat generation as a byproduct of its operation; which leads to a higher temperature and sometimes risk of failure. Therefore, thermal management of such devices is to be proper and efficient to ensure the safe operating temperature of the device components within the allowable design limit. It drives research from the last few decades, and researchers have explored several passive techniques to control thermo-fluid flow and heat transfer rate using different classical problem geometries. In this regard, the use of appropriate working fluid plays an important role. A pure fluid like air, water, ethylene glycol or mineral oils may not fulfill the design temperature limits of any device and its components. On the other hand, the addition of higher-thermal-conductivity nanoparticles such as Cu, CuO, Ag, AgO, TiO₂, Al₂O₃ and CNTs to the pure fluid (termed as nanofluid) is a promising technique for enhancing heat transfer. Despite a few unfavorable arguments, beneficial aspects using nanofluids can be found in the open literature in refs. [8–13]. Further to this, adding different types of nanoparticles to the base fluid (known as hybrid nanofluid) is a current technique in order to boost the thermal performance of conventional fluids and mono-nanofluids. This shows also a promising technique for heat transfer augmentation in numerous appliances. A review of this aspect can be found in the open literature in refs. [11, 14–16].

Different types of convective heat transfer phenomena using hybrid nanofluids in classical flow geometries have been investigated by several researchers. Evolved flow physics becomes more complicated in the presence of porous matrix and external magnetic fields under various thermal boundary conditions. The thermo-fluid behaviors and heat transfer of hybrid nanofluids in a cavity have been investigated by Ghalambaz et al. [17] considering a clear domain

and an external magnetic field, and a porous domain by Chamkha et al. [18], Ghalambaz et al. [19] and Al-Srayyih et al. [20]. On the other hand, Suresh et al. [21] conducted an experimental investigation of Cu–Al₂O₃/water hybrid nanofluid and they reported the maximum enhancement of heat transfer as ~13.56% with respect to pure water. Magnetohydrodynamic thermal convection of hybrid nanofluids in classical cavity geometry was studied in [22–27] and in many other works. All these studies have considered either isothermal or constant heat flux condition.

Despite many developments in working fluids (as stated above), the enhancement of natural convective heat transfer is challenging from industrial, energy-saving and control perspectives. In earlier published works, several basic approaches are reported for enhancing heat transfer during natural convection. In this context, the spatial heating with a sinusoidal profile plays a major role to enhance heat transfer of a thermal system. A detailed account of the review on the above has already been reported in refs. [2, 28, 29]. Natural convective heat transfer through porous media has been investigated by several authors considering sinusoidal heating at the bottom/horizontal wall(s) [30, 31], sidewalls [32, 33], etc. In other class of works, adopting sinusoidal heating condition, the convective heat transfer of a nanofluid in a clear domain has been analyzed by Mikhailenko et al. [34] and Oztop et al. [35], whereas, the cases of porous domain have been analyzed by Alsabery et al. [36], Arasteh et al. [37]. The effect of cavity shape such as sinusoidal wall [38–40] or wavy heat source [41] on natural convection heat transfer of nanofluid saturated porous media has also been reported. Magnetohydrodynamic thermal convection of nanofluid saturated porous domain subjected to a sinusoidal heating has been analyzed by Malik and Nayak [42], Nazeer et al. [43], Javaherdeh and Najjarnezami [44], Sheremet and Pop [45], Pordanjani et al. [46], etc. Vo et al. [47] have investigated magnetohydrodynamic thermal convection of nanomaterial migration in a sinusoidal porous enclosure.

Recently, Tayebi and Chamkha [48] have studied the enhancement of natural convective heat transfer of a sinusoidally heated cavity utilizing hybrid nanofluid. They reported that the use of Cu–Al₂O₃/water hybrid nanofluid is beneficial for superior heat transport in comparison to Al₂O₃/water mono-nanofluid and pure water. Effect of sinusoidally corrugated sidewalls of an enclosure on improving heat transfer rate utilizing Cu–Al₂O₃/water hybrid nanofluid has been studied by Takabi and Salehi [49]. In their study, it was observed that hybrid nanofluid is efficient for improving the heat transfer performance compared to a single type of nanofluid. Later, Ashorynejad and Shahriari [50] studied a case of MHD natural convective heat transfer in an open wavy enclosure filled with Cu–Al₂O₃/water hybrid nanofluid and reported about the positive role of this hybrid nanofluid on heat transfer enhancement. Very recently, several

researchers have studied convective heat transfer in different flow geometries utilizing hybrid nanofluids in the absence of magnetic fields [51, 52], presence of magnetic fields [53–55] and presence of both magnetic fields and porous substances [56–58].

From the survey of the relevant literature, it is clearly noted that the application of a sinusoidal heating condition in classical problem geometry applicable to thermal and engineering systems is of great interest from enhancing thermal performance as well as better control of it. Thus, the present study aims to explore magnetohydrodynamic heat transfer augmentation of Cu–Al₂O₃/water hybrid nanofluid saturated with porous enclosure subjected to multi-frequency spatial heating (following a half-sinusoidal function) undergoing natural convection. The half-sinusoidal heating condition is imposed on the bottom wall of the cavity, whereas the heated fluid in the cavity is allowed to release heat out of the cavity through the cold sidewalls. The effect of additional uniform temperature (referred as offset temperature in this work) which is superposed to the imposed sinusoidal heating is also analyzed systematically, to explore thermo-fluid flow behavior. The implementation of offset temperature and multi-frequency half-sinusoidal heating profile at different frequencies is a novel contribution in this area. In our opinion, the outcome of the study can provide an original contribution to the design and development of any devices in the scientific field.

Mathematical modeling aspects

The physical model of the proposed problem geometry is essentially a square cavity with its length scale H (such that $L=H$) as illustrated in Fig. 1a. The bottom wall of the cavity is heated nonuniformly with multi-frequency spatial heating conditions following a half-sinusoidal function and offset temperature (θ_{os}). It is important to note that the

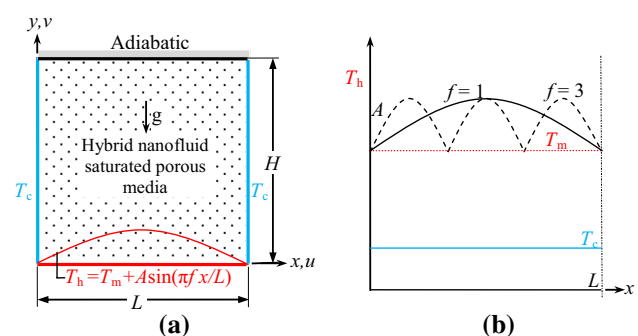


Fig. 1 (Color online) **a** Schematic diagram of the physical domain with computational boundary conditions, **b** multi-frequency spatial heating (following a half-sinusoidal function and offset temperature)

half-sinusoidal heating condition is adopted considering the mean temperature (T_m) of heating [2]. To report the efficacy in thermal performance of the multi-frequency spatially heated cavity, a case of constant isothermal heating with the same geometrical and boundary conditions is also analyzed. The top wall of the cavity is thermally insulated, whereas the sidewalls are cold at a constant temperature T_c (where $T_m > T_c$) and exchange heat with the surroundings. The cavity is packed with Cu–Al₂O₃/water hybrid nanofluid saturated porous matrix. An external magnetic field (uniformly distributed with a strength B) is applied horizontally, which affects the thermo-fluid flow behavior inside the cavity. The no-slip boundary condition at all walls of the cavity is assumed, and the walls are impermeable. Furthermore, the point of singularity at the junction of hot and cold temperatures is avoided by inserting suitable insulation patches [2].

The porous media provide resistance to the fluid flow, which in turn reduces the rate of heat transfer of the thermal system markedly. In this study, an attempt has been made to improve heat transfer which is to be reported using the heat transfer augmentation parameter. To achieve this, some datum parameters need to be considered for the comparison purpose. Here, the mean temperature of heating is adopted for the multi-frequency spatial heating (following a half-sinusoidal function) on the bottom wall of the cavity (as illustrated in Fig. 1b).

The thermal performance of the cavity is assessed by analyzing thermo-fluid behavior and the rate of heat transfer from the cavity, assuming the flow to be steady, two-dimensional, incompressible, Newtonian and laminar within the validity of the Boussinesq approximation. The porous matrix is modeled by adopting the Brinkman–Forchheimer–Darcy model (BFDM) and the local thermal equilibrium model (LTE) between fluid and porous body. It is also assumed that the porous medium is hydrodynamically and thermally homogeneous and isotropic. The viscous dissipation effect is negligible compared to the conduction and convection terms in the energy balance equation. It is also assumed to have uniform porosity and permeability throughout the cavity [1, 2, 8, 59, 60].

In this study, the hybrid nanofluid basically comprises base fluid (water) and a combination of two different nanoparticles of Cu and Al₂O₃. It is assumed that the nanoparticles (having diameter ~ 1 nm) are stable for all time and floating homogeneously in base fluid without any sedimentation or agglomeration [60, 61]. The nanoparticles are uniform in shape and size (of spherical type). The thermo-physical properties of the pure fluid ($Pr = 6.93$) and the combination of Cu and Al₂O₃ nanoparticles are assumed to be constant and are presented in Table 1 (assuming an average fluid temperature 300 K) [62]. Furthermore, it is assumed that the applied magnetic field is uniform over the entire cavity filled with electrically

Table 1 Thermo-physical properties of the pure fluid and nanoparticles (Cu and Al₂O₃) [17, 18, 21, 64]

Physical properties	Water	Cu	Al ₂ O ₃
$c_p/J\text{ kg}^{-1}\text{ K}^{-1}$	4179	385	765
$k/W\text{ m}^{-1}\text{ K}^{-1}$	0.613	401	40
$\alpha/\text{kg m}^{-3}$	1.47×10^{-7}	1.11×10^{-4}	131.7×10^{-7}
β/K^{-1}	21×10^{-5}	1.67×10^{-5}	0.85×10^{-5}
$\rho/\text{kg m}^{-3}$	997.1	8933	3970
$\mu/\text{kg m}^{-1}\text{ s}^{-1}$	9.09×10^{-4}	–	–

conducting fluid, resulting in the Lorentz force. The Joule heating and Hall effect are insignificant in the study.

Based on the above assumptions, the dimensionless governing equations for mass, momentum and energy balances can be expressed as

$$\frac{\partial U}{\partial X} + \frac{\partial V}{\partial Y} = 0 \quad (1)$$

$$\begin{aligned} & \frac{1}{\varepsilon^2} \left(U \frac{\partial U}{\partial X} + V \frac{\partial U}{\partial Y} \right) \\ &= -\frac{\rho_f}{\rho_{\text{hnf}}} \frac{\partial P}{\partial X} + \frac{v_{\text{hnf}} Pr}{v_f \varepsilon} \left(\frac{\partial^2 U}{\partial X^2} + \frac{\partial^2 U}{\partial Y^2} \right) \\ & \quad - \left(\frac{v_{\text{hnf}} Pr}{v_f Da} + \frac{F_c \sqrt{U^2 + V^2}}{\sqrt{Da} \varepsilon^{3/2}} \right) U \end{aligned} \quad (2)$$

$$\begin{aligned} & \frac{1}{\varepsilon^2} \left(U \frac{\partial V}{\partial X} + V \frac{\partial V}{\partial Y} \right) \\ &= -\frac{\rho_f}{\rho_{\text{hnf}}} \frac{\partial P}{\partial Y} + \frac{v_{\text{hnf}} Pr}{v_f \varepsilon} \left(\frac{\partial^2 V}{\partial X^2} + \frac{\partial^2 V}{\partial Y^2} \right) \\ & \quad - \left(\frac{v_{\text{hnf}} Pr}{v_f Da} + \frac{F_c \sqrt{U^2 + V^2}}{\sqrt{Da} \varepsilon^{3/2}} \right) V \\ & \quad - \frac{\rho_f}{\rho_{\text{hnf}}} \frac{\sigma_{\text{hnf}}}{\sigma_f} Ha^2 V + \frac{(\rho\beta)_{\text{hnf}}}{\rho_{\text{hnf}} \beta_f} Ra Pr \theta \end{aligned} \quad (3)$$

$$\left(U \frac{\partial \theta}{\partial X} + V \frac{\partial \theta}{\partial Y} \right) = \frac{\alpha_{\text{hnf}}}{\alpha_f} \left(\frac{\partial^2 \theta}{\partial X^2} + \frac{\partial^2 \theta}{\partial Y^2} \right) \quad (4)$$

where the dimensionless parameters are as follows. The symbol ε is the porosity of porous medium, X and Y are the coordinates, U and V are velocity component in X and Y directions, θ is the nondimensional temperature, and P is the nondimensional pressure. The fluid properties (such as density— ρ , viscosity— μ , thermal conductivity— k and volumetric expansion coefficient— β) are indicated by the subscript ‘hnf’ for the hybrid nanofluid. The evaluation of all these properties is based on volumetric concentration of hybrid nanoparticles (ϕ) in the pure liquid. Incorporating

the corresponding properties of the base fluid (as denoted by the subscript ‘f’) and the solid particles (as denoted by the subscript ‘s’), the dimensionless equations are formulated utilizing the following relations.

The effective density of hybrid nanofluid is expressed by

$$\rho_{\text{hnf}} = (1 - \phi_{\text{hnf}})\rho_f + \phi_{\text{Al}_2\text{O}_3} \rho_{\text{Al}_2\text{O}_3} + \phi_{\text{Cu}} \rho_{\text{Cu}} \tag{5}$$

where $\phi_{\text{hnf}} = \phi_{\text{Al}_2\text{O}_3} + \phi_{\text{Cu}}$

The thermal expansion coefficient (volumetric) and the specific heat capacity of hybrid nanofluid are evaluated from:

$$(\rho\beta)_{\text{hnf}} = (1 - \phi_{\text{hnf}})(\rho\beta)_f + \phi_{\text{Al}_2\text{O}_3}(\rho\beta)_{\text{Al}_2\text{O}_3} + \phi_{\text{Cu}}(\rho\beta)_{\text{Cu}} \tag{6}$$

and

$$(\rho c_p)_{\text{hnf}} = (1 - \phi_{\text{hnf}})(\rho c_p)_f + \phi_{\text{Al}_2\text{O}_3}(\rho c_p)_{\text{Al}_2\text{O}_3} + \phi_{\text{Cu}}(\rho c_p)_{\text{Cu}} \tag{7}$$

The thermal diffusivity is expressed as

$$\alpha_{\text{hnf}} = k_{\text{hnf}}/(\rho c_p)_{\text{hnf}} \tag{8}$$

The effective dynamic viscosity of the hybrid nanofluid could be computed by adopting the classical Brinkman model [61] as:

$$\mu_{\text{hnf}} = \frac{\mu_f}{(1 - \phi_{\text{hnf}})^{2.5}} \tag{9}$$

Furthermore, the effective electrical conductivity of the hybrid nanofluid is calculated following the Maxwell model [63]

$$\sigma_{\text{hnf}} = \sigma_f \left[1 + \frac{3(\sigma_s/\sigma_f - 1)\phi_{\text{hnf}}}{(\sigma_s/\sigma_f + 2) - (\sigma_s/\sigma_f - 1)\phi_{\text{hnf}}} \right] \tag{10}$$

where $\phi_{\text{hnf}}\sigma_s = \phi_{\text{Cu}}\sigma_{\text{Cu}} + \phi_{\text{Al}_2\text{O}_3}\sigma_{\text{Al}_2\text{O}_3}$

The effective thermal conductivity could be obtained by the Maxwell model [63] as

$$k_{\text{hnf}} = k_f \left[\frac{(k_s + 2k_f) - 2\phi_{\text{hnf}}(k_f - k_s)}{(k_s + 2k_f) + \phi_{\text{hnf}}(k_f - k_s)} \right] \tag{11}$$

where $\phi_{\text{hnf}}k_s = \phi_{\text{Cu}}k_{\text{Cu}} + \phi_{\text{Al}_2\text{O}_3}k_{\text{Al}_2\text{O}_3}$

where k_{Cu} , $k_{\text{Al}_2\text{O}_3}$ and k_f are, respectively, the thermal conductivities of spherical nanoparticles of Cu and Al_2O_3 and the pure fluid. However, it is observed from the experimental data [64] that the above classical models for thermal conductivity (Maxwell model) as well as viscosity (Brinkman model) are not sufficient to accurately estimate these values for Cu– Al_2O_3 /water hybrid nanofluid [17, 18, 21, 64]. For this reason, the available experimental data [64] for the thermal conductivity and viscosity of Cu– Al_2O_3 /water hybrid nanofluid are utilized in the present work and the same is presented in Table 2 for $\phi_{\text{hnf}} = 0.1\text{--}2\%$. $\phi_{\text{hnf}} = 3\%$ (as

Table 2 Effective thermal conductivity and dynamic viscosity of Cu– Al_2O_3 /water hybrid nanofluid [64]

$\phi_{\text{hnf}}/\%$	$\phi_{\text{Cu}}/\%$	$\phi_{\text{Al}_2\text{O}_3}/\%$	$k_{\text{hnf}}/\text{W m}^{-1} \text{K}^{-1}$	$\mu_{\text{hnf}}/\text{kg m}^{-1} \text{s}^{-1}$
0.1	0.0038	0.0962	0.619982	0.000972
0.33	0.0125	0.3175	0.630980	0.001098
0.75	0.0285	0.7215	0.649004	0.001386
1	0.0380	0.9620	0.657008	0.001602
2	0.0759	1.9241	0.684992	0.001935
3	0.1138	2.8862	0.712976	0.002268

indicated in the last row of Table 2) is obtained by extrapolating the data a little bit for the sake of extending this numerical study.

The present analysis is carried out in the dimensionless form. The dimensionless forms of the governing Eqs. (1)–(4) are obtained by introducing nondimensional variables as elaborated below.

$$(X, Y) = (x, y)/H;$$

$$(U, V) = (u, v)H/\alpha_f;$$

$$\theta = (T - T_c)/(T_m - T_c);$$

$$P = (p - p_a)H^2/\rho_f\alpha_f^2 \tag{12a}$$

$$\text{Pr} = \frac{\nu_f}{\alpha_f}; \quad \text{Da} = \frac{K}{H^2}; \quad F_c = \frac{1.75}{\sqrt{150}};$$

$$\text{Ra} = \frac{g\beta_f(T_m - T_c)H^3}{\nu_f\alpha_f}; \quad \text{Ra}_m = \text{RaDa}; \quad \text{Ha} = \frac{BH}{\sqrt{\nu_f\rho_f/\sigma_f}} \tag{12b}$$

where Pr, Da, F_c , Ra, Ra_m and Ha are Prandtl number, Darcy number, Forchheimer coefficient, Rayleigh number, Darcy–Rayleigh number (or modified Rayleigh number) and Hartmann number, respectively. Utilizing the following boundary conditions, the dimensionless governing Eqs. (1)–(4) are solved:

- (a) $U = V = 0, \theta = 0$ for the left cold wall ($X = 0$),
- (b) $U = V = 0, \theta = 0$ for the right cold wall ($X = 1$),
- (c) $U = V = \frac{\partial\theta}{\partial Y} = 0$ for the top adiabatic wall ($Y = 1$),
- (d) $U = V = 0, \theta = \theta_{\text{os}} + I \sin(\pi f X)$ for the heated bottom wall ($Y = 0$).

where I implies the nondimensional amplitude [$I = A/(T_m - T_c)$] of the half-sinusoidal heating profile and it can vary between 0.1 and 1. The symbol θ_{os} stands for dimensionless initial offset temperature and it varies between 0 and 1 in this study.

The rate of heat transfer from the heated bottom wall is computed in dimensionless form using the average Nusselt number (Nu) and is given by

$$Nu = \frac{k_{hnf}}{k_f} \int_0^1 \left(- \frac{\partial \theta}{\partial Y} \Big|_{Y=0} \right) dX \tag{13}$$

The fluid flow distribution within the computation domain is visualized using stream function (ψ) and corresponding streamlines. It is pertinent to note that ψ on all walls is zero. The stream function (ψ) is expressed as

$$- \frac{\partial \psi}{\partial X} = V \quad \text{and} \quad \frac{\partial \psi}{\partial Y} = U \tag{14}$$

In addition to the streamlines, the thermal energy transportation from the heat source to the heat sink is visualized utilizing heatlines. The heatlines are derived from the steady-state energy balance and generated from the heat function (Π) [65], which can be expressed as

$$- \frac{\partial \Pi}{\partial X} = V\theta - \frac{\partial \theta}{\partial Y} \quad \text{and} \quad \frac{\partial \Pi}{\partial Y} = U\theta - \frac{\partial \theta}{\partial X} \tag{15}$$

These equations are solved by adopting an integration approach applying zero surface velocity and the Dirichlet and Neumann boundary conditions for temperature. To initiate the solution, a reference point for Π is put as ‘0’ at the central point of the bottom wall ($X=0.5, Y=0$) so that a symmetrical distribution in the cavity is maintained.

Numerical procedure, grid independence test and validation study

The set of nonlinear and coupled governing Eqs. (1)–(4) is solved numerically in dimensionless form based on the finite volume approach (FVM) employing relevant boundary

conditions. The computation is carried out using an indigenous CFD code, validated extensively and reported in our earlier works [2, 28, 59, 60]. The present study is conducted using a staggered uniform grid structure, SIMPLE algorithm [66], TDMA and ADI sweep. The computations are carried out in an iterative manner minimizing the residuals ($< 10^{-8}$) of the governing equations. It is to be noted that, on the discretization of the governing equations, the second-order central differencing scheme is followed for the diffusion terms, whereas for the advection terms QUICK (a third-order upwind) scheme is adopted.

Code validation

The developed code has already been used for the validation of different types of problems [28, 59, 60] on natural and mixed convection. In our recent work [2], a validation study using a porous cavity heated nonuniformly at the bottom wall and cooled at the sidewalls has been reported. However, one more validation study is presented here using the published data of Ghasemi et al. [66] on magnetohydrodynamic natural convection of Al_2O_3 –water nanofluid in a differentially heated enclosure for $Pr=6.2, Ra=10^5$ and $Ha=0-60$. The simulated results of the average Nusselt number (Nu) and maximum stream function ($|\psi|_{max}$) with increasing Hartmann number (Ha) as presented in Table 3 are found to be closer with the published results [66]. This implies that the performance of the in-house CFD code is reliable, and the accuracy is satisfactory.

Grid independence study

Before the present computation, the mesh sensitivity to the solution of the present problem is tested by conducting a grid

Table 3 Comparison of average Nu (and $|\psi|_{max}$ in parentheses) at $Ra=10^5, Pr=6.2$, different values of Ha and ϕ

Ha	Results of Ghasemi et al. [66]			Present code results		
	$\phi=0$	$\phi=0.02$	$\phi=0.04$	$\phi=0$	$\phi=0.02$	$\phi=0.04$
0	4.738 (11.053)	4.820 (11.313)	4.896 (11.561)	4.776 (11.270)	4.857 (11.529)	4.933 (11.776)
15	4.143 (8.484)	4.179 (8.615)	4.211 (8.734)	4.168 (8.612)	4.243 (8.866)	4.314 (9.115)
30	3.150 (5.710)	3.138 (5.682)	3.124 (5.642)	3.163 (5.755)	3.221 (5.906)	3.278 (6.053)
45	2.369 (3.825)	2.342 (3.729)	2.317 (3.629)	2.377 (3.838)	2.423 (3.915)	2.468 (3.989)
60	1.851 (2.623)	1.831 (2.518)	1.815 (2.415)	1.857 (2.626)	1.897 (2.663)	1.822 (2.416)

Table 4 Mesh sensitivity analysis at $Da=10^{-4}, \epsilon=0.6, \theta_{os}=0.5, I=1, f=5, Ha=30$ and a range of Ra_m values ($10-10^4$)

Ra_m	Average Nu (successive error in %)				
	80×80	120×120	160×160	200×200	250×250
10	7.610	7.899 (3.67%)	8.104 (2.52%)	8.262 (1.92%)	8.262 (0.0%)
10^2	8.355	8.613 (2.99%)	8.802 (2.15%)	8.952 (1.68%)	8.950 (0.03%)
10^3	16.759	16.828 (0.63%)	16.936 (0.63%)	17.044 (0.63%)	17.062 (0.11%)
10^4	34.356	33.390 (2.89%)	32.963 (1.29%)	32.786 (0.54%)	32.807 (0.06%)

independence test using average Nusselt number (Nu). The mesh sensitivity is performed with five different grid sizes (80×80 , 120×120 , 160×160 , 200×200 and 250×250) for $Da = 10^{-4}$, $\varepsilon = 0.6$, $\theta_{os} = 0.5$, $I = 1$, $f = 5$, $Ha = 30$ and $Ra_m = 10\text{--}10^4$. Table 4 presents the mesh sensitivity results of the average Nu at $Y = 0$. From this analysis, it is observed that the error is found $< 1.9\%$ with 200×200 grid size compared to immediate coarse mesh. Beyond this grid size, there is no significant change in Nu value estimation. Therefore, 200×200 grid size is most appropriate for the present simulation of multi-frequency heating.

Results and discussion

The efficacy of multi-frequency spatial heating (following a half-sinusoidal function) of Cu–Al₂O₃/water hybrid nanofluid saturated porous cavity subjected to an external magnetic field is analyzed in this study. The effect of different offset temperatures (θ_{os}) on the rate of heat transfer is analyzed. The rate of heat transfer with multi-frequency spatial heating is compared to a case of isothermal heating at the bottom wall. Any augmentation in the heat transfer will be greatly beneficial for the designing of any thermal system, working on natural convection along with multi-physical conditions (porous media, nanofluid, hybrid nanofluid, magnetic field, heat generation, etc.). Both uniform and half-sinusoidal heating conditions are analyzed with the variation of Darcy–Rayleigh number $Ra_m = 10, 10^2, 10^3$ and 10^4 keeping the fixed value of Darcy number $Da = 10^{-4}$ and porosity $\varepsilon = 0.6$. The initial offset temperature is taken as $\theta_{os} = 0.1, 0.3, 0.5, 0.7$ and 1 , and the amplitude of half-sinusoidal heating varies as $I = 0.05, 0.3, 0.5, 0.7$ and 1 . The frequency of half-sinusoidal heating conditions (temperature) is chosen as $f = 1, 3, 5, 7$ and 10 . The concentration of nanoparticles varies as $\phi = 0.001\text{--}0.03$. The strength of the imposed magnetic field is varied as $Ha = 10, 30$ and 50 . All the results under different parametric conditions are analyzed in terms of contours of streamlines and isotherms, average Nu and heat transfer parameter η and presented in sections “[Summary of multi-frequency half-sinusoidal heating on heat transfer characteristics](#)”–“[Heat transfer characteristics](#).” Firstly, the efficacy of half-sinusoidal heating on the rate of heat transfer characteristics is presented for a range of multi-frequency and compared in section “[Summary of multi-frequency half-sinusoidal heating on heat transfer characteristics](#).” In section “[Effect of uniform heating and nonuniform heating on heat flow dynamics](#),” the effect of uniform and sinusoidal heating on the thermo-fluid flow structure with varying Darcy–Rayleigh numbers is illustrated. The effects of different offset temperatures as well as the amplitude of sinusoidal heating on heat flow dynamics are presented next in section “[Effect of various offset temperatures and](#)

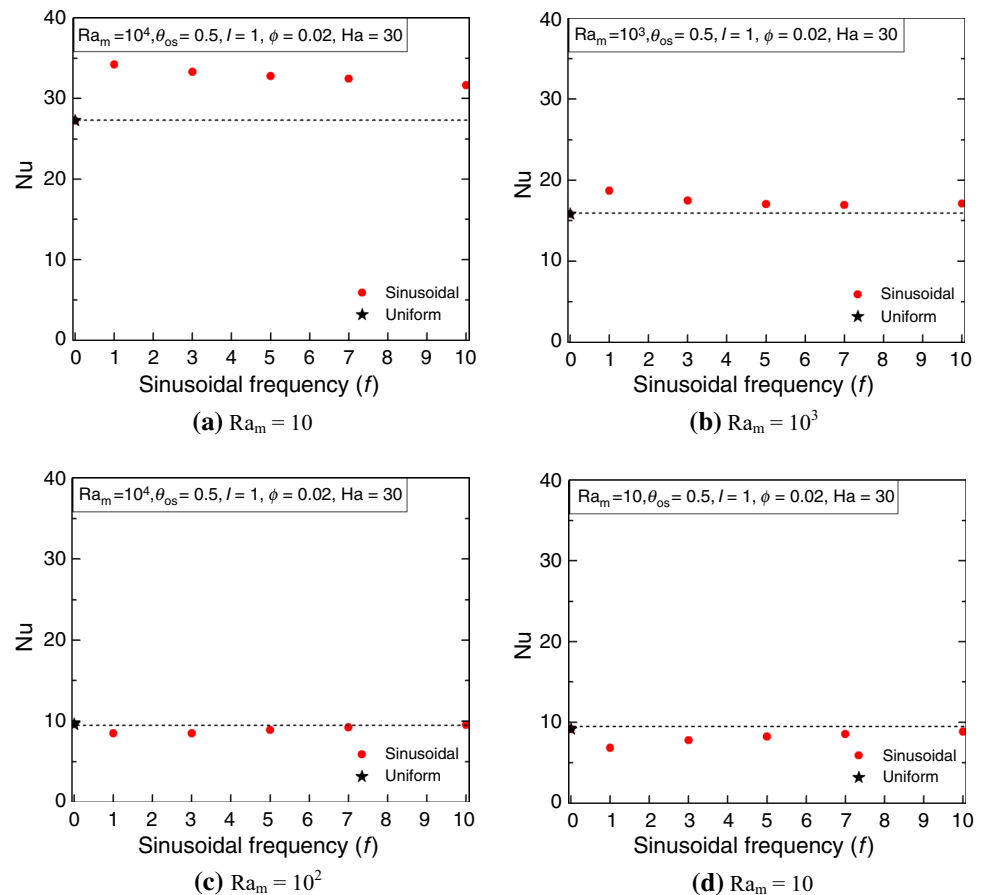
[amplitudes on heat flow dynamics under half-sinusoidal heating](#).” In section “[Effect of multi-frequency heating on heat flow dynamics](#),” the dynamics of heat and fluid flow for a range of frequencies of heating is illustrated. The impacts of different strengths of magnetic fields on the thermo-fluid flow are elaborated in section “[Impact of Hartmann number \(Ha\) on heat flow dynamics](#).” Next, section “[Effect of hybrid nanofluid volume concentration \(\$\phi\$ \) on heat flow dynamics](#)” illustrates the effects of various concentrations of hybrid nanoparticles on heat flow dynamics. Finally, the rate of heat transfer and overall thermal performance is reported in section “[Heat transfer characteristics](#).”

Summary of multi-frequency half-sinusoidal heating on heat transfer characteristics

Before conducting a detailed parametric study, the efficacy of multi-frequency spatial heating is assessed by making a comparison with the results of a uniform heating condition for the same parametric combination. The same is illustrated in Fig. 2 in terms of variation of rate of heat transfer (average Nusselt number, Nu) with the varying frequency f at $Ha = 30$, $I = 1$, $\theta_{os} = 0.5$ for Cu–Al₂O₃/water hybrid nanofluid ($\phi = 0.02$). In Fig. 2a, the average Nu with uniform heating is shown by the marker ‘*’ and by a dashed horizontal line for a better understanding of heat transfer characteristics under different parametric values. At $Ra_m = 10^4$, Fig. 2a clearly indicates the positive effect of half-sinusoidal heating and it is true for any frequency (f); it means the heat transfer rate is substantially enhanced. As the frequency of heating increases, the average Nu value decreases marginally, but a heightening rate of heat transfer is clearly noted throughout the range of studied frequencies. A similar beneficial effect of half-sinusoidal heating is noted with a lower value of $Ra_m = 10^3$ (Fig. 2b). Of course, the fluid flow dynamics as well as heat transfer characteristics inside the enclosure is totally governed by the modes of heat transfers—conduction and convection. With the higher Darcy–Rayleigh number, $Ra_m = 10^4$, convection mechanism due to buoyancy is stronger, leading to higher fluid flow velocity. Thus, a higher heat transfer rate is noted. On the other hand, at lower values, $Ra_m < 10^2$, the convection becomes weaker as the conduction mode dominates, thus lowering the fluid velocity. It leads to a decrease in Nu values; even it falls below isothermal heating condition.

It is interesting to note that at $Ra_m \leq 10^2$ as indicated in Fig. 2c, d, although Nu value is lower with sinusoidal heating compared to isothermal heating condition, the rate of heat transfer increases with the increasing frequency of sinusoidal heating. At $f = 10$ Nu reaches to the Nu value of an isothermal heating condition. The reason behind this fact is as follows. When the frequency of spatial heating increases, the temperature distribution at the bottom wall

Fig. 2 (Color online) Overview of heat transfer characteristics under multi-frequency heating conditions at $\theta_{os}=0.5$, $I=1$, $Ha=30$ for Cu–Al₂O₃/water hybrid nanofluid ($\phi=0.02$): **a** $Ra_m=10^4$, **b** $Ra_m=10^3$, **c** $Ra_m=10^2$ and **d** $Ra_m=10$



of the cavity becomes closer to that due to uniform heating. Furthermore, as the frequency of sinusoidal heating (temperature) increases, the number of points of intermediate cooling (through which heat is rejected out from the bottom wall) also increases. It results in a decrement in mean temperature of heating as well as average Nu. This fact can be easily understood from the local average Nu distribution over the bottom wall, which is presented in section “[Effect of multi-frequency heating on heat flow dynamics](#).” Hence, from this exercise, it is clearly noted that the application of half-sinusoidal heating has a positive contribution to enhance convective heat transfer, and at a higher value of Ra_m , this positive gain is much more.

Effect of uniform heating and nonuniform heating on heat flow dynamics

To get an insight into heat transfer characteristics, thermo-fluid flow structures are illustrated in Fig. 3 using streamlines (top row), isotherms (second row) and heatlines (bottom row) for both uniform heating (first and second columns) and nonuniform heating (third and fourth columns). Two different values of Darcy–Rayleigh number are considered ($Ra_m=10^4$ and 10) keeping other parameters constant

($\theta_{os}=0.5$, $I=1$, $f=1$, $\phi=0.02$). As the enclosure fluid is heated at the bottom, due to lighter density the heated fluid adjacent to the bottom wall moves upward about the central part of the cavity. The heat rejection/cooling takes place to the cold sidewalls. As a result of this, two counter-rotating circulation cells are formed symmetrically with respect to the central vertical plane of the cavity. Now, at a higher value of $Ra_m=10^4$, thermal convection becomes very strong resulting in a stronger fluid circulation compared to that at $Ra_m=10$, which can be visualized from the magnitude of the maximum values of the stream function. Comparing the streamline contours of uniform heating (first two columns) with that of nonuniform heating at $f=1$ (third and fourth columns), it is clearly noted that the nonuniform heating causes a higher strength of fluid circulation (for both Ra_m values), leading to a higher rate of heat transfer (reflected in Fig. 2b).

The distribution of isotherms adjacent to the heated wall (about the middle portion of the cavity) indicates higher temperature therein, and finally, this high-temperature zone broadens over the entire cavity. The distribution of isotherms with nonuniform heating changes significantly compared to that of uniform heating. The peak value of temperature is located at the midpoint of the bottom wall of the cavity under the half-sinusoidal heating.

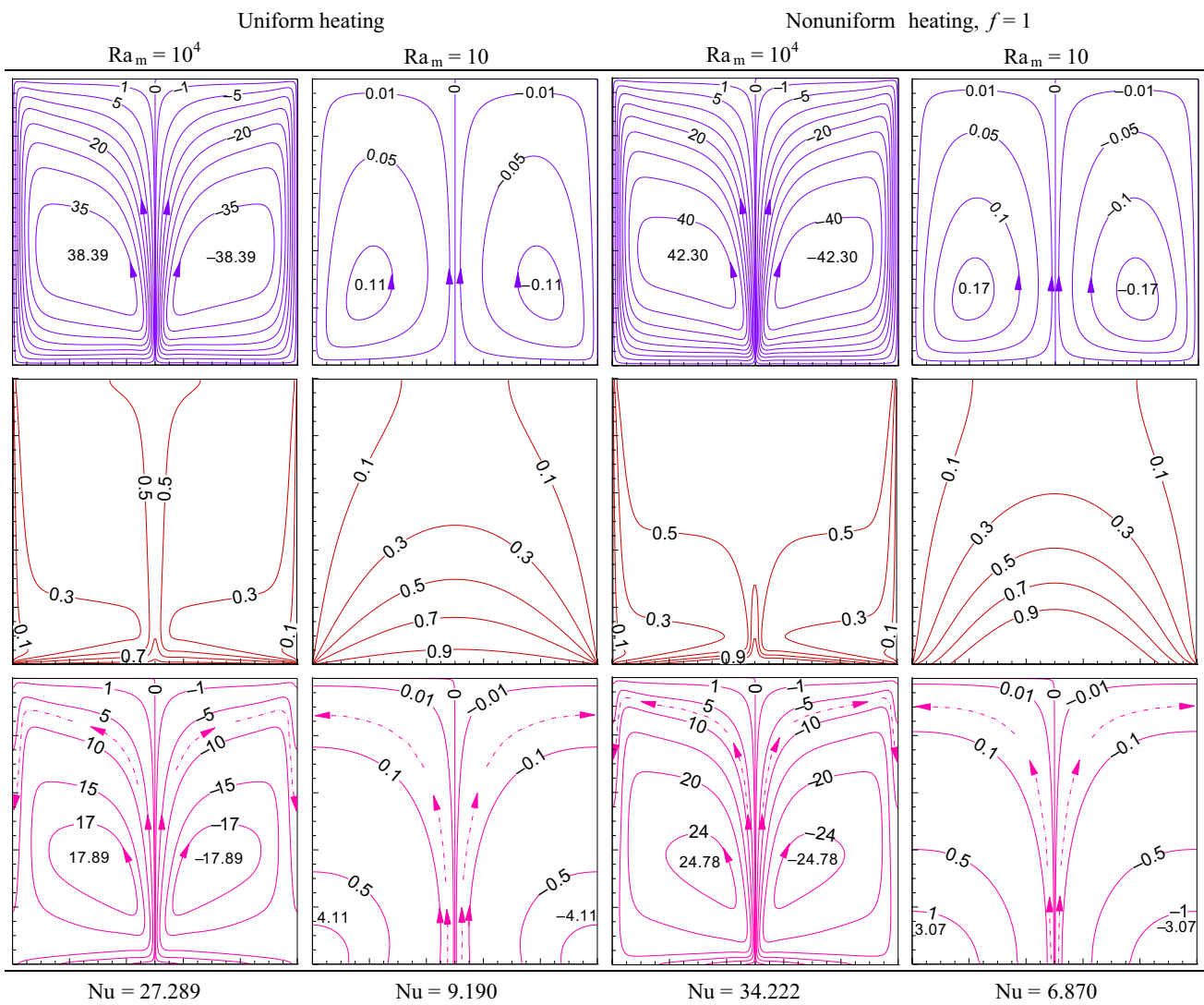


Fig. 3 (Color online) Effect of Darcy–Rayleigh number (Ra_m) on the dynamics of thermo-fluid flow structure at $Da=10^{-4}$, $Ha=30$, $\theta_{os}=0.5$, $I=1$, $f=1$ for Cu– Al_2O_3 hybrid nanofluid ($\phi=0.02$). The

contour intervals are chosen as 0.1 for isotherms, 5 for streamlines (for $Ra_m=10^4$), 0.05 (for $Ra_m=10$), 5 for heatlines (for $Ra_m=10^4$), 0.5 (for $Ra_m=10$), respectively

The heat energy transport from the heated bottom wall to the cold sidewalls is depicted using the heatline contours. It shows a direct connection between the bottom and sidewalls. As marked with the arrowheads, the heat energy is transported through the narrowed corridors (from a heat source to a heat sink) about the mid-vertical plane, and thereafter, the corridors are broadened. The heat function becomes maximum over the sidewalls. At the higher value of $Ra_m = 10^4$, convective heat flux is strong enough; thus, the intensity of the local heat flux becomes more resulting in narrowed energy corridors. This leads to the formation of two numbers of energy circulations at the lower part

of the cavity. The magnitude as well as the size of such energy circulation cells is higher due to higher-thermal-energy transportation through the energy corridors with nonuniform heating compared to that of uniform heating. At the lower $Ra_m = 10$, energy circulation cells disappear and energy transport corridors broaden as the intensity of local heat flux is lower. It is to be noted that, for the contours of both streamlines and heatlines, the clockwise (CW) rotation is designated with the negative (‘-’) sign, whereas the counterclockwise (CCW) rotation is designated with the positive (‘+’) sign before the contour values.

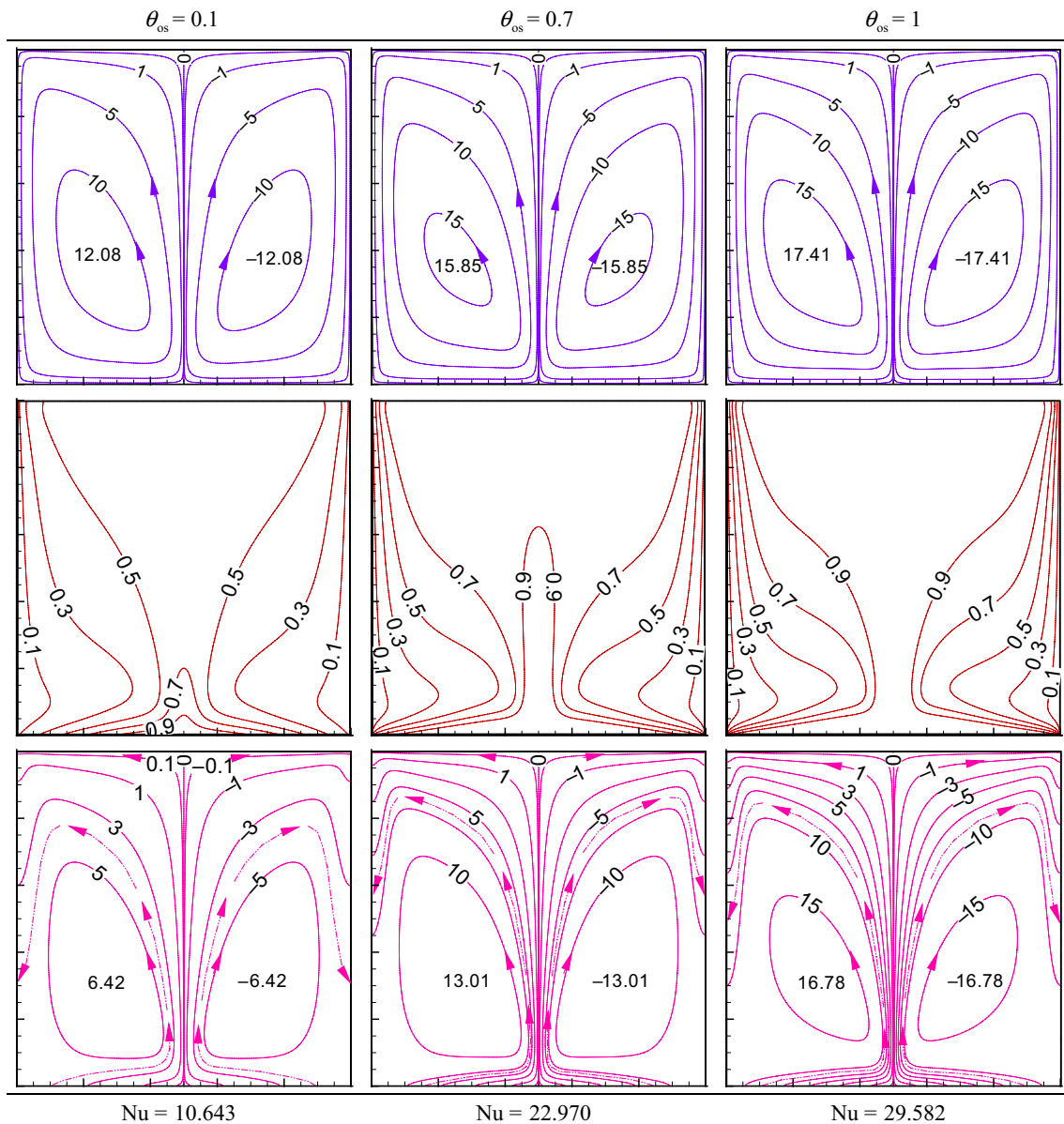


Fig. 4 (Color online) Effect of offset temperature (θ_{os}) on the dynamics of thermo-fluid flow structure at $Ra_m = 10^3$, $Ha = 30$, $I = 1$, $f = 1$ for Cu- Al_2O_3 hybrid nanofluid ($\phi = 0.02$). The contour intervals are chosen as 0.1 for isotherms, 5 for streamlines, 2 for heatlines

Effect of various offset temperatures and amplitudes on heat flow dynamics under half-sinusoidal heating

For the understanding of the consequence of offset temperature (θ_{os}) on the fluid and heat flow dynamics under the half-sinusoidal heating conditions, the contours of streamlines (first row), isotherms (second row) and heatlines (last row) are demonstrated in Figs. 4 and 5 for dimensionless offset temperature $\theta_{os} = 0.1$, 0.7 and 1 at frequencies $f = 1$ and 5, and $Ra_m = 10^3$, $Ha = 30$, $I = 1$, $\phi = 0.02$. In Fig. 4, at $f = 1$, a lower value of $\theta_{os} = 0.1$ essentially indicates

a lower mean temperature of sinusoidal heating, which means heat flux addition into the enclosure fluid is significantly lower. This can be noticed from the distribution of dimensionless temperature within the cavity, which shows lower values of isotherms over the entire cavity (except heated bottom wall). Eventually as θ_{os} increases to 0.7 and then 1, the fluid temperature near the hot wall increases significantly following the nonuniform heating pattern and the heating is spreading up to the upper part of the cavity. The temperature gradients at bottom wall and sidewalls become higher as reflected by corresponding isotherms. It is pertinent with the increasing θ_{os} value

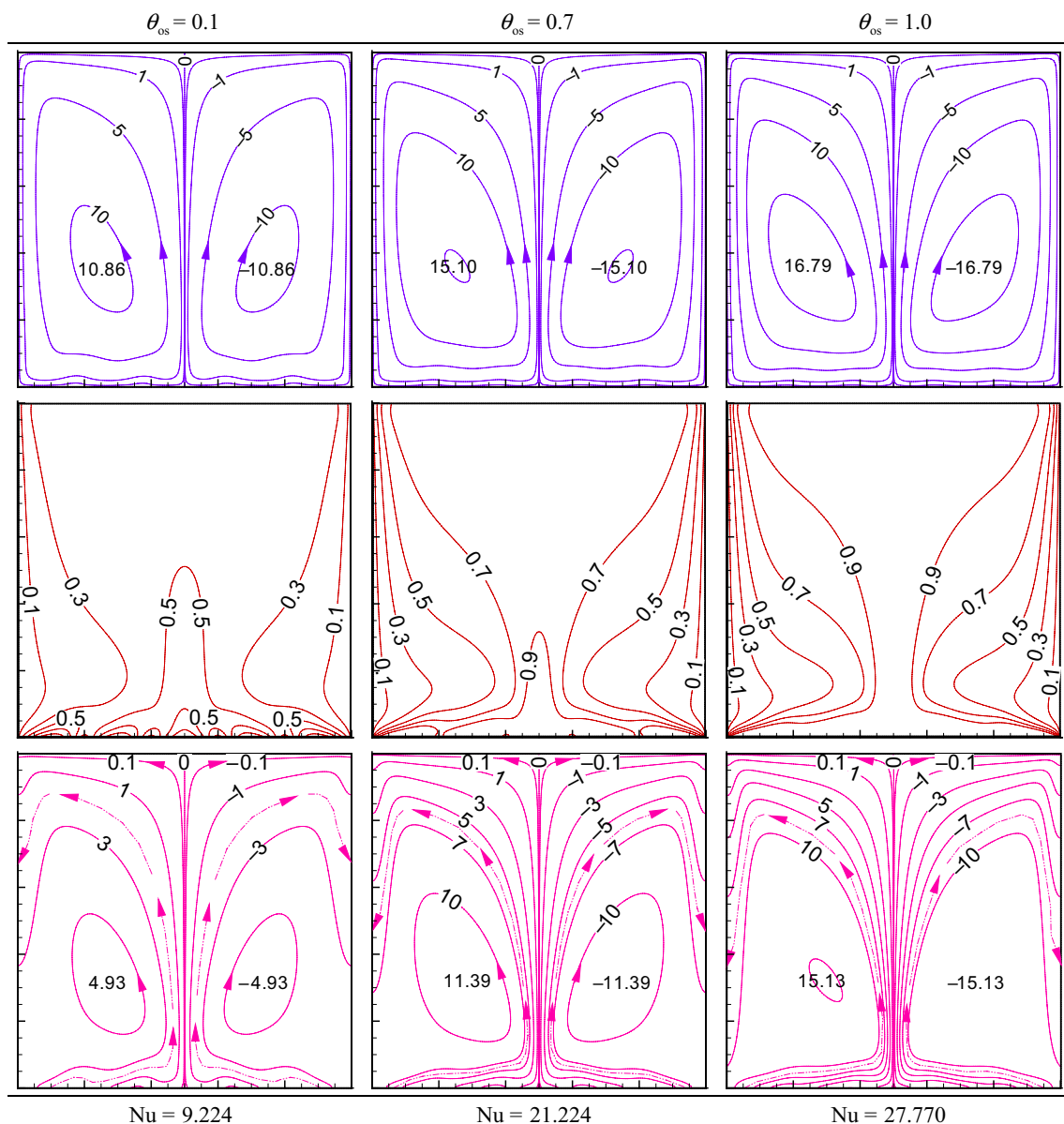


Fig. 5 (Color online) Effect of offset temperature (θ_{os}) on the dynamics of thermo-fluid flow structure at $Ra_m = 10^3$, $Ha = 30$, $I = 1$, $f = 5$ for Cu- Al_2O_3 hybrid nanofluid ($\phi = 0.02$). The contour intervals are chosen as 0.1 for isotherms, 5 for streamlines, 2 for heatlines

that, as the fluid temperature increases the strength of the fluid circulation also increases. It leads to a higher rate of transport of thermal energy from the bottom heated wall to the cold sidewalls. It results in an increased Nu value. A single isothermal peak exists about the mid-vertical plane. The corresponding contours of heatlines differ strength-wise significantly. Symmetrical distribution about the mid-vertical plane is maintained for both the fluid and energy circulation cells. The ψ_{max} and Π_{max} is maximum at $\theta_{os} = 1$; it is due to a higher mean temperature of sinusoidal heating. Corresponding magnitude of the heat transfer rate (Nu) increases markedly compared to that of uniform

heating condition. However, for higher frequency $f = 5$ as in Fig. 5, the fluid temperature (θ) near the bottom wall differs strongly from the case of single-frequency sinusoidal heating ($f = 1$). There exists a small localized flow structure near the bottom wall, resulting in a wavy pattern in thermal and fluid flow structures. However, the strengths of fluid and energy circulations, ψ_{max} and Π_{max} , decrease at the higher frequency of sinusoidal heating (as observed earlier in Fig. 2b). It is interesting to note that the average Nu also decreases at a higher frequency. Of course, the increasing trend of Nu is clearly noted for both the frequencies ($f = 1$ and 5) as θ_{os} increases. As the temperature

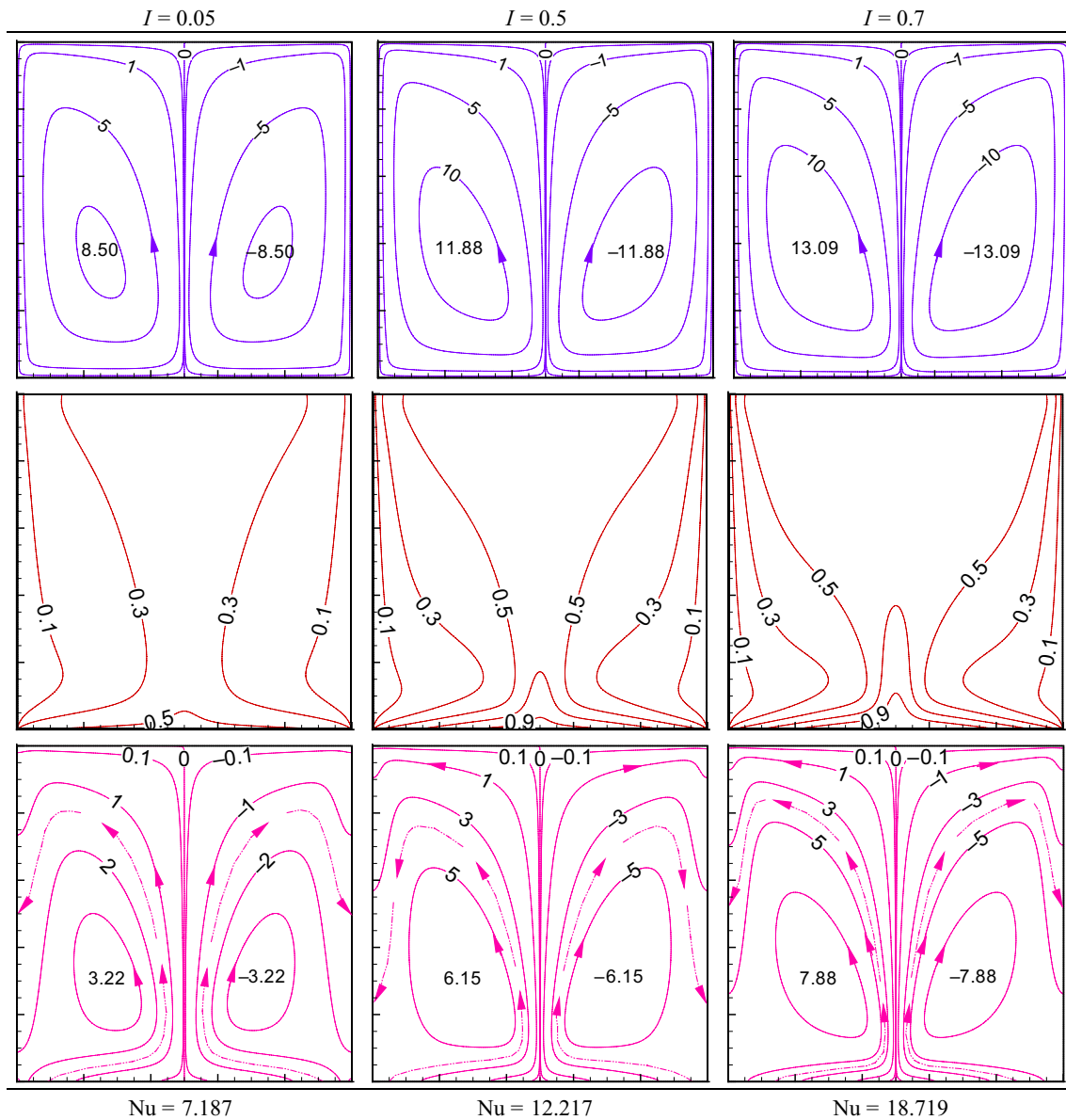


Fig. 6 (Color online) Impact of amplitude of sinusoidal heating (I) on fluid flow and thermal behavior at $Ra_m = 10^3$, $Ha = 30$, $\theta_{os} = 0.5$, $f = 1$ for Cu- Al_2O_3 hybrid nanofluid ($\phi = 0.02$). The contour intervals are chosen as 0.1 for isotherms; 5 for streamlines; 2 for heatlines

peak in the middle of the cavity becomes stronger with the increasing θ_{os} , this causes an increase in Nu value.

Furthermore, the dynamics of thermo-fluid flow alters significantly depending upon the dimensionless amplitude (I) of sinusoidal heating keeping, the parameters of θ_{os} and f fixed. To understand this effect, the contours of streamlines, isotherms and heatlines are presented in Figs. 6 and 7 for varying amplitude $I = 0.05, 0.5$ and 0.7 . Two different frequencies, $f = 1$ and 5 , are considered with fixed values of $Ra_m = 10^3$, $Ha = 30$, $\theta_{os} = 0.5$, $\phi = 0.02$. In Fig. 6, at $f = 1$, for a lower amplitude $I = 0.05$, the temperature contours indicate a distribution of lower temperature within the entire cavity. Even the peak temperature at the bottom middle point shows

the value of 0.5. It is interesting to note that, as the amplitude is very small, the mean temperature is almost closed to the temperature of uniform heating at $\theta = 0.5$. The corresponding heatline contours shows wider and weaker corridors of thermal energy transport from the hot bottom wall to cold sidewalls.

At the same frequency, when the amplitude of sinusoidal heating increases from 0.05 to 0.5, the dimensionless temperature (θ) shows a significant increment (equal to 1) near the middle point of the bottom wall. Due to an increase in the temperature gradients at the hot and cold walls, the strength of fluid circulation as well as energy circulation increases substantially. It results in an increase in ψ_{max} , Π_{max} and the

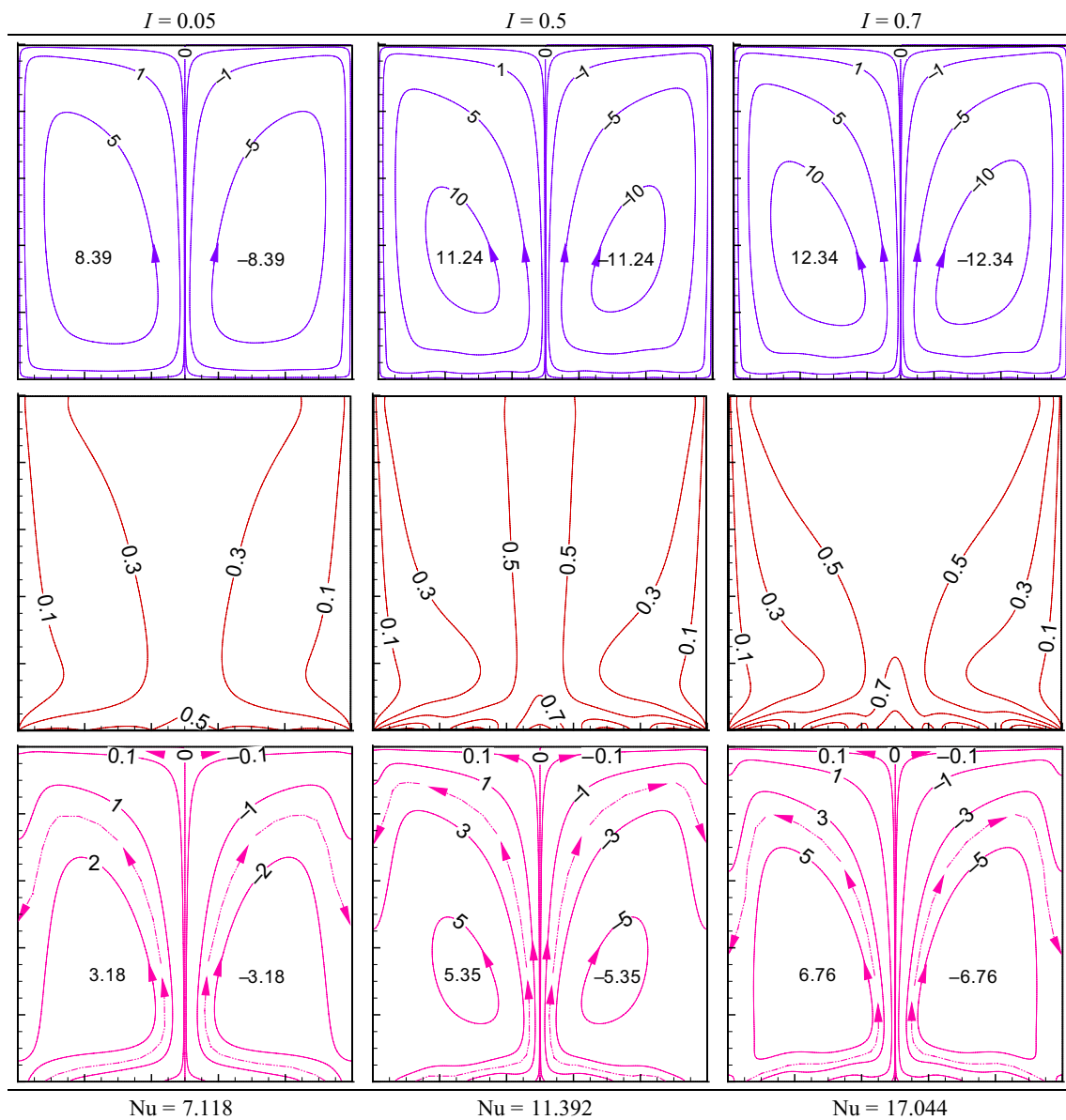


Fig. 7 (Color online) Impact of amplitude of sinusoidal heating (I) on fluid flow and thermal behavior at $Ra_m = 10^3$, $Ha = 30$, $\theta_{os} = 0.5$, $f = 5$ for Cu- Al_2O_3 hybrid nanofluid ($\phi = 0.02$). The contour intervals are chosen as 0.1 for isotherms; 5 for streamlines; 2 for heatlines

heat transfer rate. With the further increase in $I = 1.0$, the thermo-fluid flow structure is markedly changed and the rate of heat transfer also increases significantly. Of course, both the fluid and energy circulation patterns remain symmetrical. The monotonous growths in the circulation strengths (ψ_{max} , Π_{max}) along with the increasing I are noted. It also results in a growing average Nu.

The aforementioned heat and fluid flow dynamics alters especially near the bottom wall when the frequency increases to $f = 5$, keeping other parameters fixed, as shown in Fig. 7. However, the peak values of ψ_{max} and Π_{max} , and the average Nu decreased marginally compared to those of single-frequency half-sinusoidal heating ($f = 1$). It happens so due

to the formation of a wavy pattern of a thermal boundary layer near to the sinusoidally heated bottom wall. Depending upon the imposed thermal boundary conditions, the nonuniform input of thermal energy into the cavity fluid takes place (similar to Fig. 2b).

Effect of multi-frequency heating on heat flow dynamics

The effect of multi-frequency of sinusoidal heating on the heat fluid flow dynamics is analyzed for three different frequencies $f = 3, 5$ and 10 and presented for $Ra_m = 10^3$, $Ha = 30$, $\theta_{os} = 0.5$, $I = 1$ and $\phi = 0.02$ in Fig. 8. It shows an

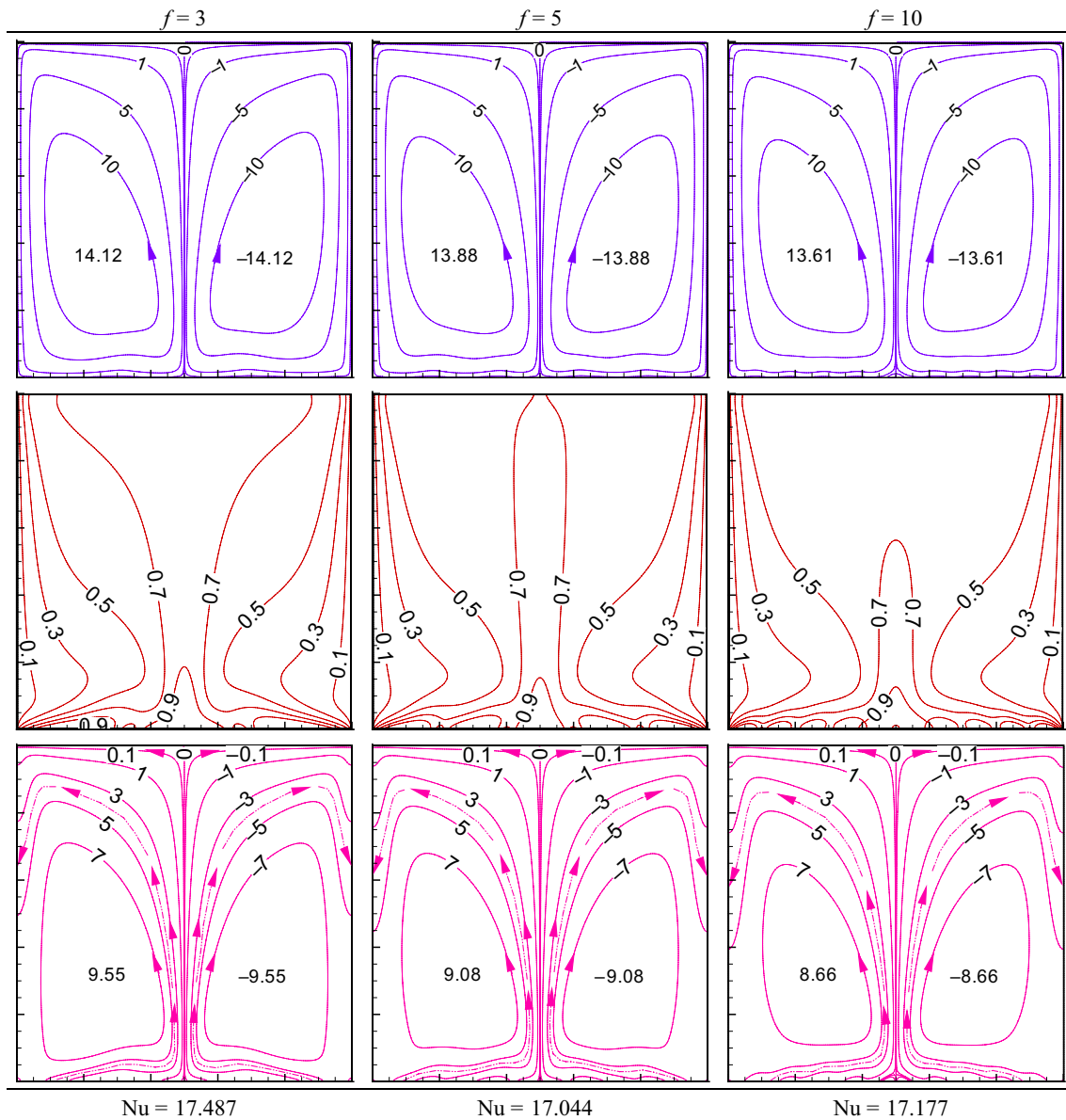


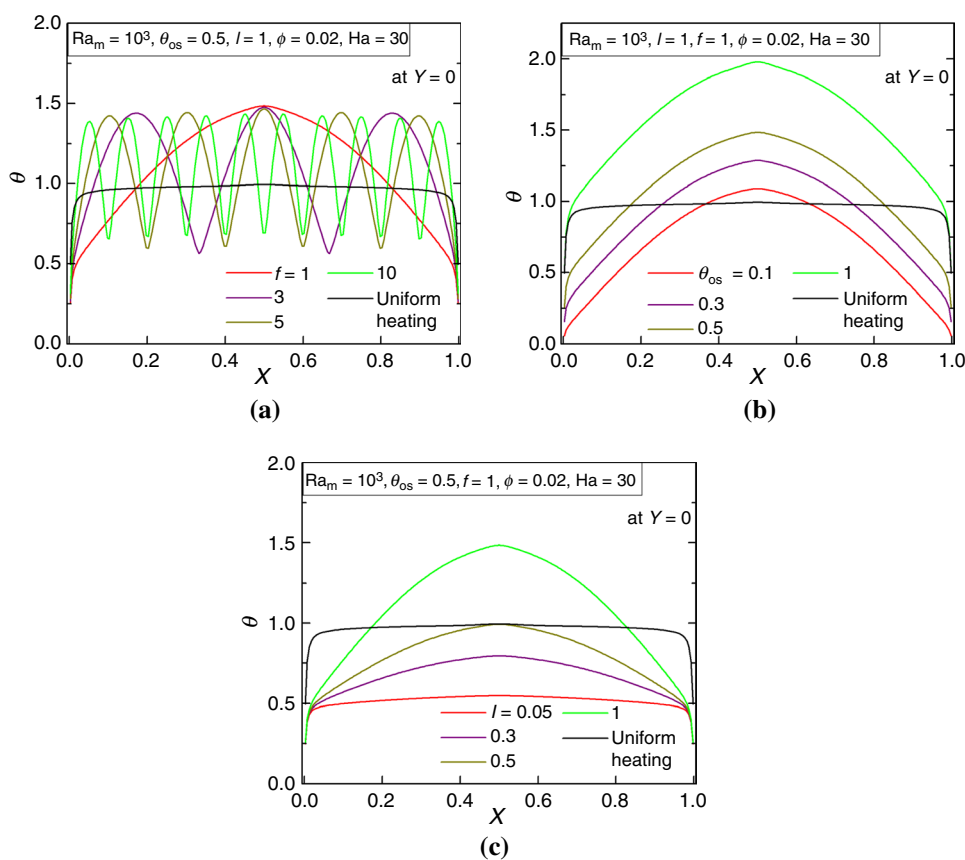
Fig. 8 (Color online) Impact of frequency of half-sinusoidal heating (f) on fluid flow and thermal behavior at $Ra_m=10^3$, $Ha=30$, $\theta_{os}=0.5$, $I=1$ for Cu–Al₂O₃ hybrid nanofluid ($\phi=0.02$). The contour intervals are chosen as 0.1 for isotherms; 5 for streamlines; 2 for heatlines

increasing frequency (beyond $f=1$) the overall fluid flow structure does not alter significantly except near to the heated bottom wall. Both the streamlines and isotherms are prominently modulated near the bottom wall with the variation of frequency. As the frequency increases, the isotherm lines nearest the bottom wall show multiple peaks and a complex flow structure. Of course, the symmetry of the flow circulation remains unaltered. From the contour lines, it is observed that tiny flow vortices are formed as the frequency increases and the formation of such flow vortices are a function of half-sinusoidal frequency. The effects of frequency variation are also clearly reflected in the contours of isotherms and heatlines. As the bottom wall is heated nonuniformly, the

temperature also varies following a half-sinusoidal function. As a result of this, the temperature pattern near the bottom wall varies spatially along its length with a temperature of high and low values in an alternate manner. As the frequency increases, such an undulation pattern increases, resulting in a decrease in the strength of fluid as well as energy circulation (as reflected in the values of ψ_{max} , Π_{max} and average Nu).

Previously, Fig. 2 shows that the multi-frequency half-sinusoidal heating is beneficial compared to uniform heating, the rate of heat transfer is guided by the thermal conditions of the half-sinusoidal heating. To understand this fact, it is of utmost importance to analyze dimensionless temperatures distribution and pattern of the local average Nusselt

Fig. 9 (Color online) Variation of dimensionless local temperature (θ) under the effect of **a** frequency (f), **b** offset temperature (θ_{os}) and **c** amplitude (I) for the fixed values of $Ra_m = 10^3$, $\phi = 0.02$ and $Ha = 30$



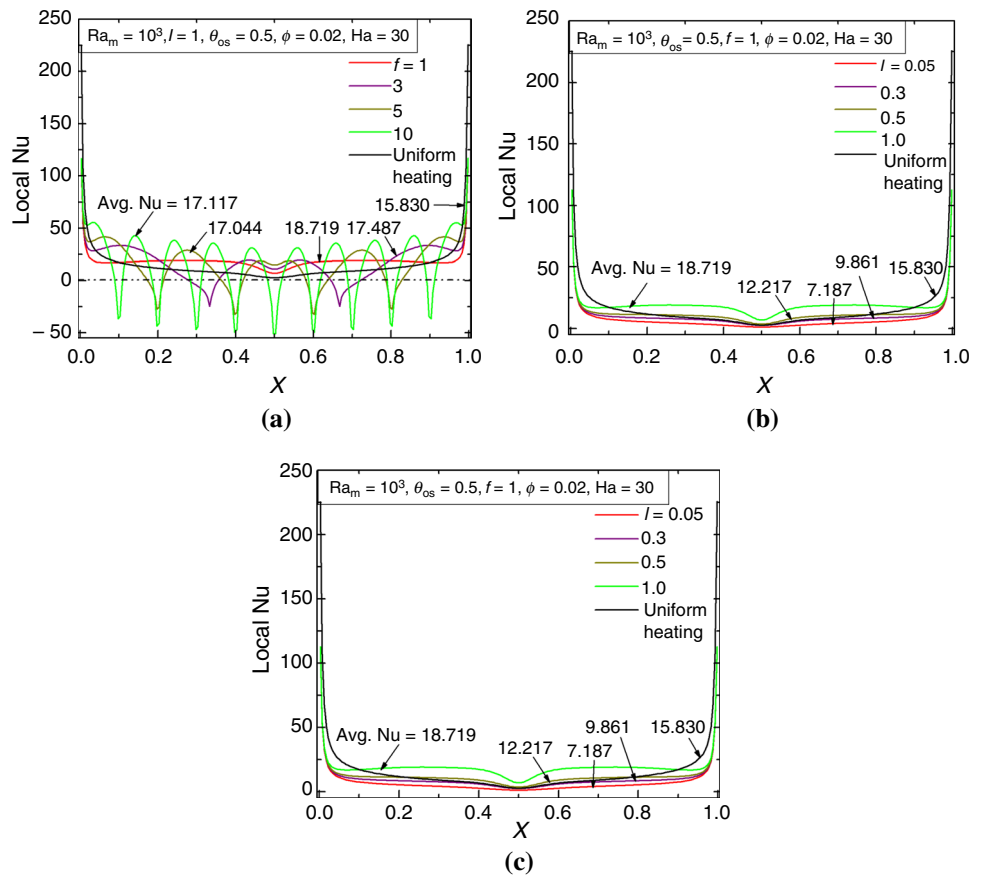
number at the heated bottom wall. It is illustrated in Figs. 9 and 10, respectively, under different parametric conditions. Figure 9a displays dimensionless temperatures (θ) distribution at the heated wall (immediate node of the wall at $Y=0$) for the fixed values of $Ra_m = 10^3$, $\theta_{os} = 0.5$, $I = 1$, $\phi = 0.02$ and $Ha = 30$. With the uniform heating profile, it clearly reflects an almost horizontal line of temperature with a value equal to 1. With the nonuniform heating condition, the dimensionless temperature at frequency $f=1$ shows a peak value (equal to 1.5) about the mid-central plane of the cavity. This temperature gradually decreases toward the cold sidewalls (due to heat rejection). When the dimensionless temperature varies between 0.5 and 1.5, the mean temperature of heating is maintained at 1. The presence of higher temperature peaks causes a higher fluid velocity inside the cavity. It leads to a higher rate of heat removal, which is reflected by the higher magnitude of Nu value. When the frequency f increases to 3, the isotherm plot shows three peak temperatures (varying between 0.5 and 1.5) over the bottom wall. Furthermore, there appear two more low-temperature points (of 0.5) due to half-sinusoidal heating condition; it leads to a reduction in thermal energy transport and heat transfer rate (as reflected by Nu). Furthermore, with an increase in frequency $f=5$ and 10, the number of low-temperature points becomes more (4 and 9, respectively), and it leads to further reduction in the

rate of heat transfer. Hence, it is obvious that the frequency of half-sinusoidal heating plays a vital role in overall thermal performance under nonuniform heating conditions.

Now, the effect of offset temperature θ_{os} on the local temperature distribution is analyzed and illustrated in Fig. 9b at fixed values of $Ra_m = 10^3$, $f = 1$, $I = 1$, $\phi = 0.02$ and $Ha = 30$. Figure 9b shows that for the same frequency of half-sinusoidal heating, the temperature magnitude for the maximum and minimum peaks is governed by θ_{os} value. At the lower value of $\theta_{os} = 0.1$, the peak temperature is significantly low, leading to a lesser temperature gradient inside the cavity as well as a lower rate of heat transfer. The increase in θ_{os} to 0.3, 0.5 and 1 leads to upward shifting of the peaks of the maximum and minimum temperature. It results in an increase in temperature gradient in the cavity causing higher circulation velocity and heat transfer. Thus, the setting of the offset temperature θ_{os} can be a means for controlling the thermal performance of the sinusoidally heated application.

On the other hand, the amplitude of the half-sinusoidal heating condition has significant influence on the magnitude of peak temperatures, which in turn affects the rates of heat transfer. To analyze this fact, the dimensionless temperature over the heated bottom wall is plotted in Fig. 9c for the fixed values of $Ra_m = 10^3$, $\theta_{os} = 0.5$, $f = 1$, $\phi = 0.02$ and $Ha = 30$. At the lower amplitude, $I = 0.05$, the temperature distribution

Fig. 10 (Color online) Variation of local Nusselt number (Nu) under the effect of **a** frequency (f), **b** offset temperature (θ_{os}) and **c** amplitude (I) for the fixed values of $Ra_m = 10^3$, $\phi = 0.02$ and $Ha = 30$



show almost a flat line with $\theta = 0.5$ (due to the imposition of $\theta_{os} = 0.5$). As the amplitude increases to $I = 0.3, 0.5$ and 1 , the temperature distribution shows an increasing trend for peak temperatures following the half-sinusoidal heating profile. Interestingly, the peak temperature reaches the temperature (equal to 1) of uniform heating condition. When $I = 0.5$ and beyond this, the peak temperature increases significantly (up to 1.5) leading to an increase in the rate of heat transfer compared to that of uniform heating condition. Thus, it appears that the half-sinusoidal heating can provide more heat transfer superior to uniform heating when $I > 0.5$ keeping other parameters fixed.

The effect of the above parametric variation on the global heat transfer excites to investigate the distribution of the local Nu along the heated bottom wall, which is illustrated in Fig. 10 for the fixed values of $Ra_m = 10^3$, $\phi = 0.02$ and $Ha = 30$. The variation of the local Nu for different f values is plotted in Fig. 10a for $\theta_{os} = 0.5$, $I = 1$. The local Nu distribution along the bottom wall follows the patterns of imposed thermal condition of half-sinusoidal heating. At the single frequency $f = 1$, the local Nu curve remains above the local Nu of uniform heating. This reflects the fact of enhanced heat transfer with nonuniform heating. However, as the frequency of half-sinusoidal heating increases to $f = 3$, there appear two more points through which heat is rejected

through the bottom wall. This implies that, with the half-sinusoidal heating, both heating and cooling take place at the bottom wall of the cavity when $f > 1$. Due to the presence of intermediate cooling zones along the bottom wall, the local Nu decreases markedly. At the sidewalls, the local Nu rises sharply—this is due to large temperature gradients with the cold sidewalls. The local Nu oscillates persistently as f increases from 1 to 10 . The peak values of the local Nu are consistently higher with the higher frequencies. Of course, the area of the cooling zones also increases with increasing f . Although the average Nu (as marked in the plot) decreases marginally with increasing f , it remains higher compared to that of uniform heating condition. It happens due to the suppression of positive heating benefit by negative intermediate cooling that appears periodically following the half-sinusoidal profile.

The local Nu is also examined under the effect of different offset temperatures and amplitudes as illustrated in Fig. 10b, c, respectively, for the fixed values of $Ra_m = 10^3$, $f = 1$, $\phi = 0.02$ and $Ha = 30$. It is observed that for the same frequency, the magnitude of average Nu increases significantly when the offset temperature increases from 0.05 to $\theta_{os} = 0.3, 0.5$ and 1 . The increased θ_{os} leads to an increase in the temperature gradient and thus a higher rate of heat transfer (as marked by the average Nu value). However, the

multi-frequency spatial heating is only advantageous (over uniform heating), when $\theta_{os} > 0.3$. The reason behind this fact is that as θ_{os} increases the mean temperature of nonuniform heating increases gradually (as observed in Fig. 9b). The maximum heat transfer rate is noted at $\theta_{os} = 1$. On the other hand, amplitude I significantly modulates the local Nu distribution, which in turn modifies the heat transfer rate. The variation of the local Nu along the bottom wall is plotted in Fig. 10c for the fixed values of $Ra_m = 10^3$, $\theta_{os} = 0.5$, $f = 1$, $\phi = 0.02$ and $Ha = 30$. At the lower amplitude I , the average Nu is lesser compared to that of uniform heating. However, with increasing amplitude beyond $I > 0.5$, the local Nu shifts upward due to a higher rate of thermal energy transfer from

the heated wall to the cavity fluid. This leads to an enhanced heat transfer as compared to the case of uniform heating condition.

Impact of Hartmann number (Ha) on heat flow dynamics

Figure 11 shows the effect of dimensionless Hartmann number ($Ha = 0, 30$ and 50) on the thermo-fluid flow fields keeping other parameters fixed at $Ra_m = 10^3$, $\theta_{os} = 0.5$, $I = 1$, $f = 1$ and $\phi = 0.02$. The corresponding results are compared against the results of a nonmagnetic case (as marked with $Ha = 0$, in the first column). It is observed that as the

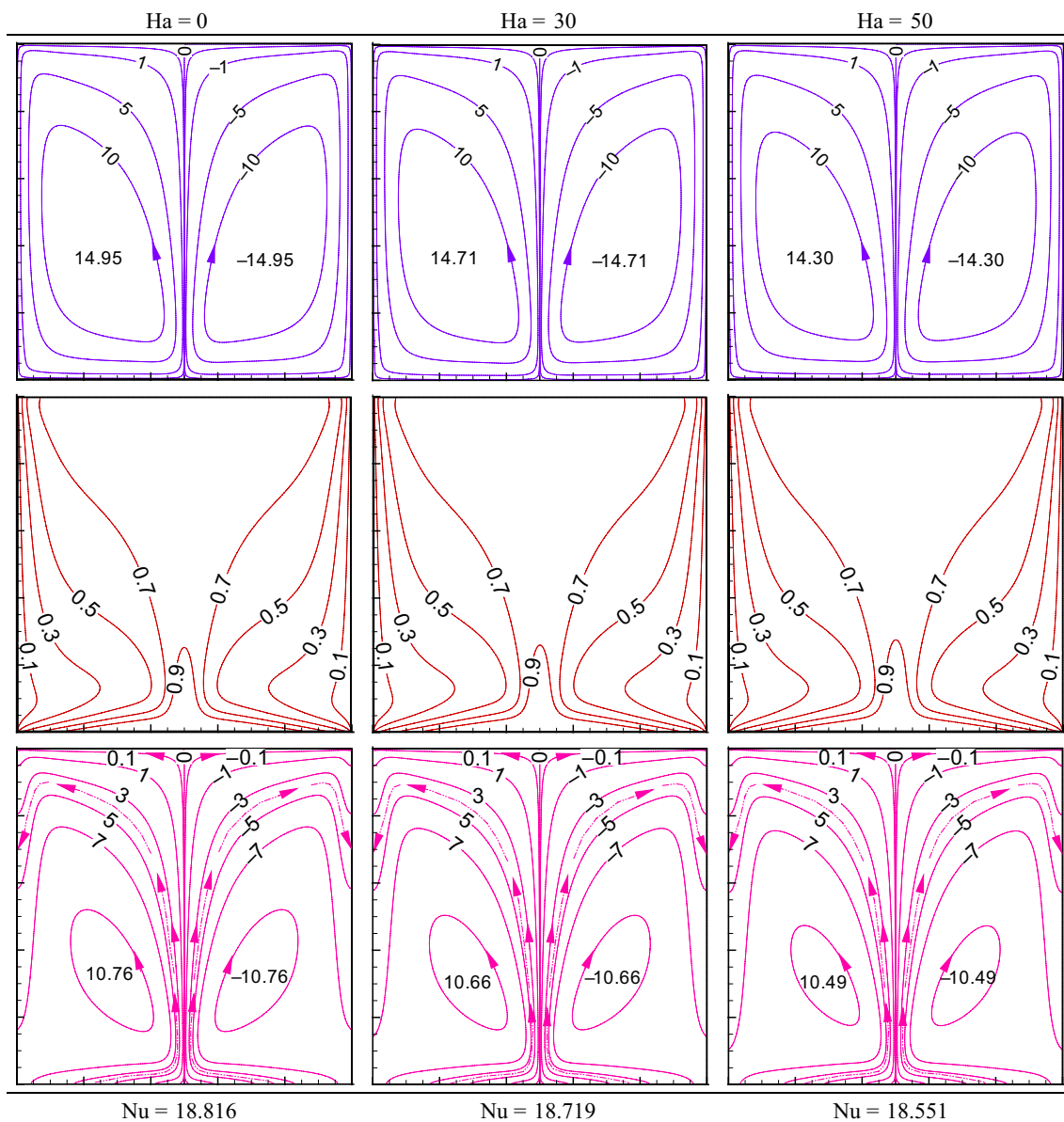


Fig. 11 (Color online) Effect of Hartmann number (Ha) on the dynamics of thermo-fluid flow structure at $Ra_m = 10^3$, $\theta_{os} = 0.5$, $I = 1$, $f = 1$ for Cu- Al_2O_3 hybrid nanofluid ($\phi = 0.02$). The contour intervals are chosen as 0.1 for isotherms; 5 for streamlines; 2 for heatlines

magnetic field strength increases the distribution of the streamlines and isotherms alters compared to no magnetic field. In the absence of the magnetic field, the strength of the circulation of hybrid nanofluid fluid becomes stronger. With the increase in Ha , the fluid circulation in the cavity decreases. The reason for such reduction can be understood from the momentum Eq. (3), where the negative source term containing Ha is present. With increasing Ha , both the U and V velocities decrease following the continuity equation. It attributes to the reduction in flow velocity as well as thermal energy transport as given in Eq. (4). In turn, it weakens the energy circulation strength and a less amount of energy is

transported from the heated bottom wall to the cold side-walls. This is reflected by ψ_{\max} , Π_{\max} and average Nu values.

Effect of hybrid nanofluid volume concentration (ϕ) on heat flow dynamics

Figure 12 illustrates the thermo-fluid flow structure of the base fluid ($\phi=0$) and two different volume concentrations ($\phi=0.001$ and 0.03) under multi-frequency half-sinusoidal heating condition at $Ra_m = 10^3$, $\theta_{os} = 0.5$, $I = 1$, $f = 3$ and $Ha = 30$. The streamlines, isotherms and heatlines show symmetrical distribution about the mid-plane of the cavity.

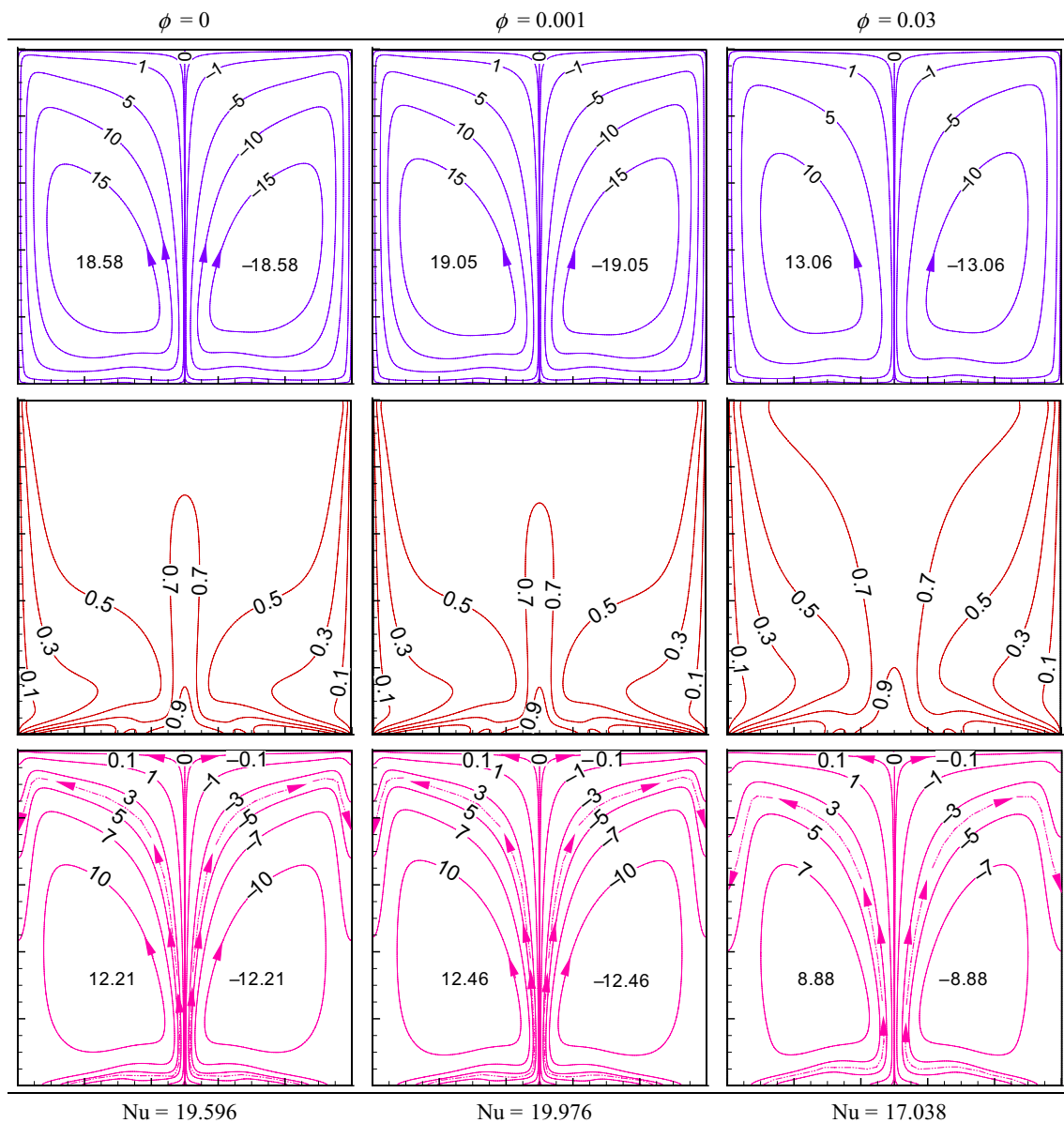


Fig. 12 (Color online) Effect of $Cu-Al_2O_3$ hybrid nanoparticle concentration (ϕ) on fluid flow and thermal behavior at $Ra_m = 10^3$, $\theta_{os} = 0.5$, $I = 1$, $f = 3$ and $Ha = 30$. The contour intervals are chosen as 0.1 for isotherms; 5 for streamlines; 2 for heatlines

Figure 12 shows that the influence of the volume fraction parameter of the hybrid nanofluid has no prominent effect on the contours of the streamlines, isotherms and heatlines. However, the addition of 0.001 Cu–Al₂O₃ nanoparticles to the base liquid results in a substantial increment in the rate of heat transfer as compared to that of the base fluid ($\phi=0$). The reason behind such increment is due to the fact that with the addition of Cu–Al₂O₃ two nanoparticles, the effective thermal conductivity increases significantly [64], in spite of the negative effect of reduced flow velocity due to enhanced viscosity. The isotherm lines are distorted significantly and deflected toward the cold sidewalls. However, when hybrid

nanoparticles concentration becomes to 0.03 (or more), a decreasing trend of heat transfer as well as fluid circulation is observed as reflected by the average Nu and ψ_{\max} values. Also the addition of the nanoparticles into the base fluid dislocates the streamlines, isotherms and heatlines as well. Of course, the gain in the effective dynamic viscosity with the presence of different combinations of nanoparticles induces more resistance to the fluid motion through the increased shear stresses. It results in a reduction in the fluid flow velocities. In turn, as the fluid velocity reduces, a reduction in the overall rate of heat transfer happens. Similar

Fig. 13 (Color online) Heat transfer characteristics with fixed values of $Ha=30$ for the variation of Ra_m (a, b), θ_{os} (c, d) and l (e, f)

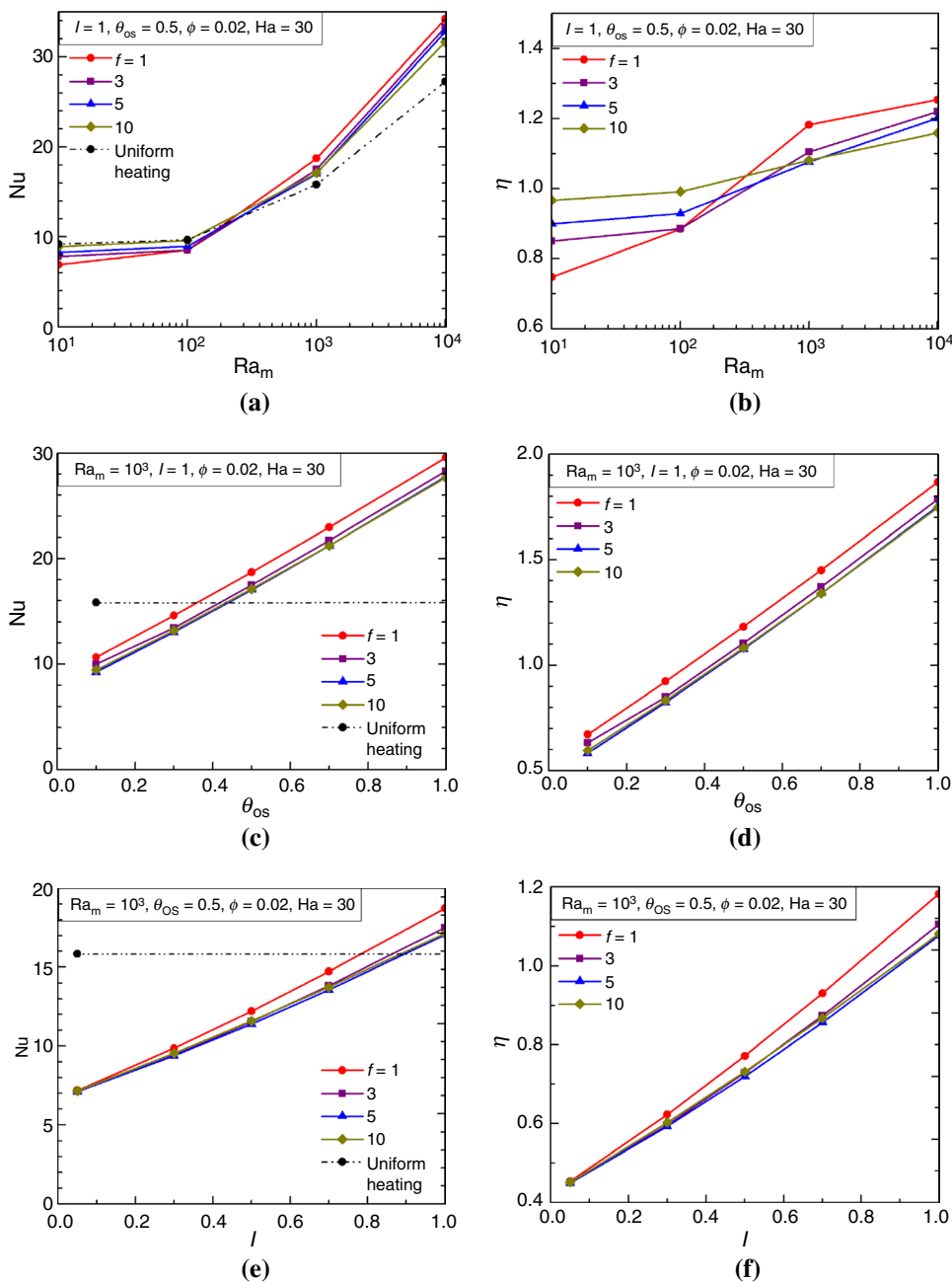
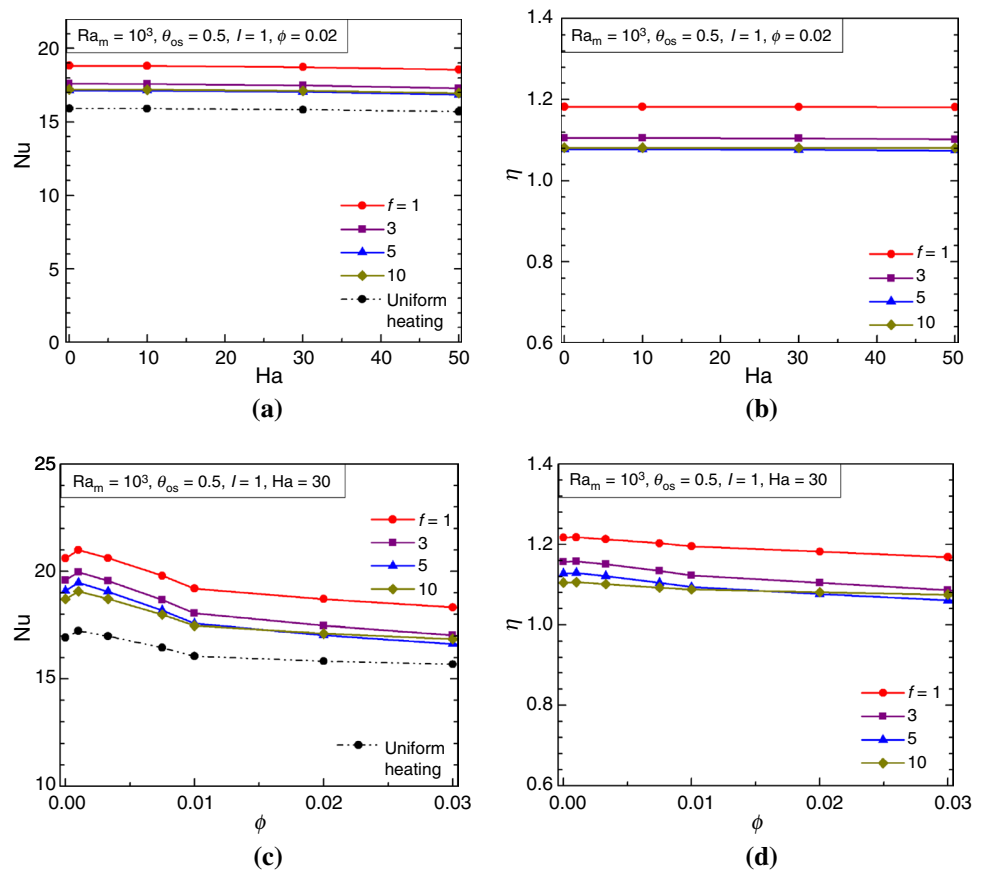


Fig. 14 (Color online) Heat transfer characteristics with the fixed values of $Ra_m = 10^3$, $\theta_{os} = 0.5$, $I = 1$ for the variation of Ha (a, b) and ϕ (c, d)



findings on hybrid nanofluids have also been reported by many researchers [48–59, 64].

Heat transfer characteristics

After conducting a number of simulations, by varying different parameters the data have been generated for the extensive analysis of the thermo-fluid flow behavior. The benefit of multi-frequency spatial heating over uniform heating of the hybrid nanofluid saturated with porous substrate is assessed and the same is illustrated in Figs. 13 and 14. The assessment of better thermal performance is estimated by defining a parameter η (termed as heat transfer parameter) as

$$\eta = \frac{Nu_{\text{sinusoidal heating}}}{Nu_{\text{isothermal heating}}} \quad (16)$$

When η is greater than 1.0, it implies an enhancement. The percentage of enhancement is $(\eta - 1) \times 100\%$. Both the average Nu and η variations under different parameters are illustrated systematically in Figs. 13 and 14.

The characteristics of Nu with Ra_m as in Fig. 13a clearly show no variation up to $< Ra_m$; thereafter, a consistently increasing pattern of Nu is noted for the constant values of $\theta_{os} = 0.5$, $I = 1$ and $Ha = 30$. A similar trend is

noted for both uniformly and nonuniformly heated conditions. It is noteworthy to mention that at a lower Ra_m , the conduction mode of heat transfer dominates over the convection, resulting in a constant trend of Nu curve. This trend is similar for the case of nonuniform heating irrespective of any frequency. Furthermore, all the Nu curves (both uniform heating and multi-frequency half-sinusoidal heating) overlap each other up to $Ra_m < 200$. Afterward, an increasing trend of Nu is observed, which is higher with half-sinusoidal heating $f = 1$. In general, the lower frequency of half-sinusoidal heating is found to be more favorable at the lower Ra_m value. For better understanding, the magnitude of the heat transfer parameter η is depicted in Fig. 13b. The heat transfer enhancement could be achieved as ~ 15.90 – 25.41% (when $\theta_{os} = 0.5$, $I = 1$, $Ha = 30$, $\phi = 0.02$). The imposed multi-frequency heating at the bottom wall modifies the thickness of the thermal boundary layer (with increasing frequency) due to the intermediate points of heat rejection from the bottom wall. In general, multi-frequency heating is always beneficial at higher Darcy–Rayleigh numbers, $Ra_m > 200$.

During the multi-frequency spatial heating, the dimensionless offset temperature (θ_{os}) and amplitude (I) of sinusoidal heating (temperature) play vital roles in global thermal performance. Figure 13c–f illustrates the variation of Nu as

well as η for the increasing value of θ_{os} and I for different frequencies $f=1, 3, 5, 10$ with the fixed value of $Ra_m=10^3$, $\phi=0.02$ and $Ha=30$. The average Nu value increases monotonically with the increase in θ_{os} for the different f values. A similar increasing trend is noted for the Nu plot with I . Of course, the multi-frequency sinusoidal heating is beneficial compared to uniform heating when sinusoidal offset temperature $\theta_{os}=0.5$. When $Ra_m=10^3$, $I=1$, $\phi=0.02$ and $Ha=30$, the heat transfer enhancement at $\theta_{os}=1$ is in the order of 86.88, 78.76, 75.43 and 74.78% for $f=1, 3, 5$ and 10, respectively. With regard to amplitude, after $I=0.8$, the positive contribution from the half-sinusoidal heating is significant. The maximum value of heat transfer enhancement at $I=1$ for $Ra_m=10^3$, $\theta_{os}=1$, $\phi=0.02$ and $Ha=30$ is 18.25, 10.47, 7.67 and 8.14% for $f=1, 3, 5$ and 10, respectively.

In Fig. 14, the overall thermal characteristics with regard to magnetic field (in Fig. 14a, b) and the concentration of Cu-Al₂O₃ hybrid nanofluids (in Fig. 14c, d) are presented for frequency $f=1, 3, 5, 10$, keeping $Ra_m=10^3$, $\theta_{os}=0.5$ and $I=1$ fixed. In any case, a single frequency of nonuniform heating shows maximum enhancement. As magnetic field strength increases, the rate of heat transfer decreases and a similar decreasing trend is noted for all the half-sinusoidal frequencies. Although the heat transfer enhancement for the range of $Ha=0-50$ and $Ra_m=10^3$, $\theta_{os}=0.5$, $I=1$ and $\phi=0.02$ are observed in the range of 7.47–18.28%. The addition of Cu-Al₂O₃ hybrid nanoparticles into the base fluid shows significant enhancement of heat transfer—21.82, 18.84, 12.95 and 10.63% for $f=1, 3, 5$ and 10, respectively, at $\phi=0.001$ (when $Ra_m=10^3$, $\theta_{os}=0.5$, $I=1$ and $Ha=30$). The maximum enhancement of heat transfer is obtained at $\phi=0.001$ and the heat transfer parameter reduces markedly up to $\phi=0.03$. For any frequency of half-sinusoidal heating, the gain in heat transfer is only noted at $\phi=0.001$ (compared to base liquid) and further increase in concentration of hybrid nanoparticles has no positive gain. It is interesting to note that for any frequency, the half-sinusoidal heating is always superior with any nanoparticles concentration (ϕ) compared to uniform heating.

Conclusions

In this work, an approach for enhancing steady-state magnetohydrodynamic natural convection heat transfer of hybrid nanofluid saturated porous medium heated nonuniformly has been demonstrated. The efficacy of half-sinusoidal heating superposed with a uniform temperature (offset temperature) is examined utilizing a classical square flow geometry heated at bottom, cooled at sides and packed with Cu-Al₂O₃/water hybrid nanofluid saturated porous medium in the presence of an external magnetic field. The coupled nonlinear governing equations are solved in dimensionless forms using

an in-house CFD code based on the finite volume approach. The study is conducted for a wide range of parametric impacts to analyze global heat transfer performance such as the variations in amplitude (I), offset temperature (θ_{os}), frequency of half-sinusoidal heating and Darcy-Rayleigh number (Ra_m). Furthermore, the concentration of Cu-Al₂O₃ hybrid nanoparticles on heat transfer rate is analyzed. The salient observations from the investigation are listed below.

- The application of multi-frequency spatial heating can lead to substantially enhanced natural convective heat transfer over the uniform heating even in the presence of flow dampening porous substrate and magnetic field.
- The heat energy transfer from the heat source to the heat sink under various thermal conditions within the cavity is visualized and explained using heatlines.
- The frequency of repetition of half-sinusoidal heating (temperature) is explored up to $f=1-10$ and a positive contribution to the heat transfer enhancement is observed at $f=1$. At a higher value of Ra_m , the gain is as high as 25.41% (when $\theta_{os}=0.5$, $I=1$, $Ha=30$, $\phi=0.02$) compared to the uniform heating. In general, multi-frequency heating is always beneficial at higher $Ra_m > 200$.
- As the frequency of half-sinusoidal heating (temperature) increases beyond $f=1$, both heating and cooling take place at the bottom wall of the cavity and the local Nu oscillates persistently as f increases from 1 to 10. Due to the presence of intermediate cooling zones, the local Nu decreases markedly, but it remains higher compared to the case of uniform heating.
- For the multi-frequency spatial heating, the dimensionless offset temperature (θ_{os}) and amplitude (I) play vital roles in global thermal performance. The heat transfer enhancements are in the order of 74.78–86.88% for the studied range of θ_{os} (when $Ra_m=10^3$, $I=1$, $Ha=30$, $\phi=0.02$). The setting of suitable values for θ_{os} and I could be an effective means for controlling the thermal performance.
- The heat transfer enhancement by using Cu-Al₂O₃/water hybrid nanofluid could be maximum 21.82% at $\phi=0.001$ (when $Ra_m=10^3$, $\theta_{os}=0.5$, $I=1$ and $Ha=30$). A higher concentration of nanoparticles increases viscosity and more resistance to the fluid flow, leading to a reduction in the overall heat transfer.
- With the increase in the strength of the magnetic field (in terms of Ha), the rate of heat transfer decreases monotonously as the thermal buoyancy decreases.

The studies reveal that the multi-frequency spatial heating along with hybrid nanofluid can be utilized as a powerful means to improve the thermal performance of a system even with the presence of flow dampening porous

media and magnetic fields. Further to this, a proper setting of offset temperature, amplitude and frequency of half-sinusoidal heating (temperature) can control the overall thermal performance of the system. Such a novel approach can easily be adapted during the designing of any thermal devices subjected to other multi-physical systems.

Compliance with ethical standards

Conflict of interest The authors declare that they have no conflict of interest.

References

- Nield DA, Bejan A. Convection in porous media. 3rd ed. Berlin: Springer; 2006.
- Manna NK, Biswas N, Mahapatra PS. Convective heat transfer enhancement: effect of multi-frequency heating. *Int J Numer Methods Heat Fluid Flow*. 2019;29(10):3822–56.
- Garimella SV, Persoons T, Weibel JA, Gektin V. Electronics thermal management in information and communications technologies: challenges and future directions. *IEEE Trans Comp Pack Manufac Technol*. 2016;PP:1–15.
- Incropera FP. Convection heat transfers in electronic equipment cooling. *J Heat Transf*. 1988;110:1097–111.
- Remsburg R. Thermal design of electronic equipment. Boca Raton: CRC Press LLC; 2001.
- Çebi A, Celen A, Donmez AH, Karakoyun Y, Celen P, Celtek MS, Dalkılıç AS, Taner T, Wongwises S. A review of flow boiling in mini and microchannel for enhanced geometries. *J Therm Eng*. 2018;4(3):2037–74.
- Dalkılıç AS, Çelen A, Çebi A, Taner T, Wongwises S. Parametric study of energy, exergy and thermoeconomic analyses on vapor compression system cascaded with Libr/Water and NH₃/Water absorption cascade refrigeration cycle. *Anadolu Univ J Sci Technol A Appl Sci Eng*. 2017;18(1):78–96.
- Khanafer K, Vafai K. Applications of nanofluids in porous medium. *J Therm Anal Calorim*. 2019;135:1479–92.
- Babar H, Ali HM. Airfoil shaped pin-fin heat sink: potential evaluation of ferric oxide and titania nanofluids. *Energy Conv Manag*. 2019;202:112194–1–19.
- Sajid MU, Ali HM, Sufyan A, Rashid D, Zahid SU, Rehman WU. Experimental investigation of TiO₂-water nanofluid flow and heat transfer inside wavy minichannel heat sinks. *J Therm Anal Calorim*. 2019;137:1279–94.
- Kasaieian A, Daneshazarian R, Mahian O, Kolsi L, Chamkha AJ, Wongwises S, Pop I. Nanofluid flow and heat transfer in porous media: a review of the latest developments. *Int J Heat Mass Transf*. 2017;107:778–91.
- Rahimi A, Saeed AD, Kasaieipoor A, Malekshah EH. A comprehensive review on natural convection flow and heat transfer: the most practical geometries for engineering applications. *Int J Numer Method Heat Fluid Flow*. 2018;29(3):834–77.
- Nazari MA, Ghasempour R, Ahmadi MH. A review on using nanofluids in heat pipes. *J Therm Anal Calorim*. 2019;137:1847–55.
- Sarkar J, Ghosh P, Adil A. A review on hybrid nanofluids: recent research, development and applications. *Renew Sustain Energy Rev*. 2015;43:164–77.
- Bhosale GH, Borse SL, Pool Boiling CHF. Enhancement with Al₂O₃-CuO/H₂O hybrid nanofluid. *Int J Eng Res Technol*. 2013;2(10):946–50.
- Selvakumar P, Suresh S. Use of Al₂O₃-Cu/water hybrid nanofluid in an electronic heat sink. *IEEE Trans Compon Packag Manuf Technol*. 2012;2(10):1600–7.
- Ghalambaz M, Mehryan SAM, Izadpanahi E, Chamkha AJ, Wen D. MHD natural convection of Cu-Al₂O₃ water hybrid nanofluids in a cavity equally divided into two parts by a vertical flexible partition membrane. *J Therm Anal Calorim*. 2019;138:1723–43.
- Chamkha AJ, Sazegar S, Jamesahar E, Ghalambaz M. Thermal non-equilibrium heat transfer modeling of hybrid nanofluids in a structure composed of the layers of solid and porous media and free nanofluids. *Energies*. 2019;12:541.
- Ghalambaz M, Sheremet MA, Mehryan SAM, Kashkooli FM, Pop I. Local thermal non-equilibrium analysis of conjugate free convection within a porous enclosure occupied with Ag-MgO hybrid nanofluid. *J Therm Anal Calorim*. 2019;135:1381–98.
- Al-Sratty BM, Gao S, Hussain SH. Natural convection flow of a hybrid nanofluid in a square enclosure partially filled with a porous medium using a thermal non-equilibrium model. *Phys Fluids*. 2019;31:043609.
- Suresh S, Venkitaraj K, Selvakumar P, Chandrasekar M. Effect of Al₂O₃-Cu/water hybrid nanofluid in heat transfer. *Exp Therm Fluid Sci*. 2012;38:54–60.
- Mehryan SAM, Sheremet MA, Soltani M, Izadi M. Natural convection of magnetic hybrid nanofluid inside a double-porous medium using two-equation energy model. *J Mol Liq*. 2019;277:959–70.
- Izadi M, Mohebbi R, Delouei AA, Sajjadi H. Natural convection of a magnetizable hybrid nanofluid inside a porous enclosure subjected to two variable magnetic fields. *Int J Mech Sci*. 2018;151:154–69.
- Mansour MA, Siddiq S, Gorla RSR, Rashad AM. Effects of heat source and sink on entropy generation and MHD natural convection of Al₂O₃-Cu/water hybrid nanofluid filled with square porous cavity. *Therm Sci Eng Prog*. 2018;6:57–71.
- Ghadikolaei SS, Hosseinzadeh Kh, Hatami M, Ganji DD. MHD boundary layer analysis for micropolar dusty fluid containing Hybrid nanoparticles (Cu Al₂O₃) over a porous medium. *J Mol Liq*. 2018;268:813–23.
- Ghadikolaei SS, Gholinia M. Terrific effect of H₂ on 3D free convection MHD flow of C₂H₆O₂-H₂O hybrid base fluid to dissolve Cu nanoparticles in a porous space considering the thermal radiation and nanoparticle shapes effects. *Int J Hydrog Energy*. 2019;44:17072–83.
- Mehryan SAM, Izadi M, Namazian Z, Chamkha AJ. Natural convection of multi-walled carbon nanotube-Fe₃O₄/water magnetic hybrid nanofluid flowing in porous medium considering the impacts of magnetic field-dependent viscosity. *J Therm Anal Calorim*. 2019;138:1541–55.
- Biswas N, Mahapatra PS, Manna NK. Merit of non-uniform over uniform heating in a porous cavity. *Int J Heat Mass Transf*. 2016;78:135–44.
- Khandelwal MK, Bera P, Chakrabarti A. Influence of periodicity of sinusoidal bottom boundary condition on natural convection in porous enclosure. *Int J Heat Mass Transf*. 2012;55:2889–900.
- Saeid NF. Natural convection in porous cavity with sinusoidal bottom wall temperature variation. *Int Commun Heat Mass Transf*. 2005;32:454–63.
- Chandra H, Bera P, Sharma AK. Natural convection in a square cavity filled with an anisotropic porous medium due to sinusoidal heat flux on horizontal walls. *Numer Heat Transf A*. 2020;77(3):317–41.
- Cimpean DS, Revnic C, Pop I. Natural convection in a square inclined cavity filled with a porous medium with sinusoidal

- temperature distribution on both side walls. *Transp Porous Med.* 2019;130:391–404.
33. Wu F, Wang G, Zhou W. Buoyancy induced convection in a porous cavity with sinusoidally and partially thermally active sidewalls under local thermal non-equilibrium condition. *Int Commun Heat Mass Transf.* 2016;75:100–14.
 34. Mikhailenko SA, Sheremet MA, Pop I. Convective heat transfer in a rotating nanofluid cavity with sinusoidal temperature boundary condition. *J Therm Anal Calorim.* 2019;137:799–809.
 35. Oztop HF, Abu-Nada E, Varol Y, Al-Salem K. Computational analysis of nonisothermal temperature distribution on natural convection in nanofluid filled enclosures. *Super Micro.* 2011;49:453–67.
 36. Alsabery AI, Chamkha AJ, Saleh H, Hashim I, Chanane B. Effects of finite wall thickness and sinusoidal heating on convection in nanofluid saturated local thermal non-equilibrium porous cavity. *Phys A.* 2017;470:20–38.
 37. Arasteh H, Mashayekhi R, Goodarzi M, Motaharpour SH, Dahari M, Toghraie D. Heat and fluid flow analysis of metal foam embedded in a doublelayered sinusoidal heat sink under local thermal non-equilibrium condition using nanofluid. *J Therm Anal Calorim.* 2019;138:1461–76.
 38. Li Z, Shehzad SA, Sheikholeslami M. An application of CVFEM for nanofluid heat transfer intensification in a porous sinusoidal cavity considering thermal non-equilibrium model. *Comput Methods Appl Mech Eng.* 2018;339:663–80.
 39. Al-Amir QR, Ahmed SY, Hamzah HK, Ali FH. Effects of Prandtl number on natural convection in a cavity filled with Silver/Water nanofluid-saturated porous medium and non-Newtonian fluid layers separated by sinusoidal vertical interface. *Arab J Sci Eng.* 2019;44:10339–54.
 40. Aly AM, Ahmed SE, Raizah ZAS. Double-diffusive natural convection in a square porous cavity with sinusoidal distributions sidewalls filled with a nanofluid. *J Porous Media.* 2018;21(2):101–22.
 41. Aly AM, Raizah ZAS. Incompressible smoothed particle hydrodynamics method for natural convection of a ferrofluid in a partially layered porous cavity containing a sinusoidal wave rod under the effect of a variable magnetic field. *AIP Adv.* 2019;9:105210-1–21.
 42. Malik S, Nayak AK. MHD convection and entropy generation of nanofluid in a porous enclosure with sinusoidal heating. *Int J Heat Mass Transf.* 2017;111:329–45.
 43. Nazeer M, Ali N, Javed T. Numerical simulation of MHD flow of micropolar fluid inside a porous inclined cavity with uniform and non-uniform heated bottom wall. *Can J Phys.* 2018;96:576–93.
 44. Javaherdeh K, Najjarnezami A. Lattice Boltzmann simulation of MHD natural convection in a cavity with porous media and sinusoidal temperature distribution. *Appl Math Mech Engl Ed.* 2018;39(8):1187–200.
 45. Sheremet MA, Pop I. Natural convection in a square porous cavity with sinusoidal temperature distributions on both side walls filled with a nanofluid: buongiorno's mathematical model. *Transp Porous Med.* 2014;105:411–29.
 46. Pordanjani AH, Jahanbakhshi A, Nadooshan AA, Afrand M. Effect of two isothermal obstacles on the natural convection of nanofluid in the presence of magnetic field inside an enclosure with sinusoidal wall temperature distribution. *Int J Heat Mass Transf.* 2018;121:565–78.
 47. Vo DD, Shah Z, Sheikholeslami M, Shafee A, Nguyen TK. Numerical investigation of MHD nanomaterial convective migration and heat transfer within a sinusoidal porous cavity. *Phys Scr.* 2019;94:115225-1–10.
 48. Tayebi T, Chamkha AJ. Buoyancy-driven heat transfer enhancement in a sinusoidally heated enclosure utilizing hybrid nanofluid. *Comput Therm Sci.* 2017;9(5):405–21.
 49. Takabi B, Salehi S. Augmentation of the heat transfer performance of a sinusoidal corrugated enclosure by employing hybrid nanofluid. *Adv Mech Eng.* 2014;6:147059.
 50. Ashorynejad HR, Shahriari A. MHD natural convection of hybrid nanofluid in an open wavy cavity. *Results Phys.* 2018;9:440–55.
 51. Ghalambaz M, Doostani A, Izadpanahi E, Chamkha AJ. Conjugate natural convection flow of Ag–MgO/water hybrid nanofluid in a square cavity. *J Therm Anal Calorim.* 2020;139:2321–36.
 52. Almeshaal MA, Kalidasan K, Askri F, Velkenedy R, Alsagri AS, Kolsi L. Three-dimensional analysis on natural convection inside a T-shaped cavity with water-based CNT–aluminum oxide hybrid nanofluid. *J Therm Anal Calorim.* 2020;139:2089–98.
 53. Tayebi T, Chamkha AJ. Entropy generation analysis due to MHD natural convection flow in a cavity occupied with hybrid nanofluid and equipped with a conducting hollow cylinder. *J Therm Anal Calorim.* 2020;139:2165–79.
 54. Ali A, Saleem S, Mumraiz S, Saleem A, Awais M, Marwat DNK. Investigation on TiO₂–Cu/H₂O hybrid nanofluid with slip conditions in MHD peristaltic flow of Jeffrey material. *J Therm Anal Calorim.* 2020. <https://doi.org/10.1007/s10973-020-09648-1>.
 55. Shafee A, Bhatti MM, Muhammad T, Kumar R, Nam ND, Babazadeh H. Simulation of convective MHD flow with inclusion of hybrid powders. *J Therm Anal Calorim.* 2020. <https://doi.org/10.1007/s10973-020-09601-2>.
 56. Abdel-Nour Z, Aissa A, Mebarek-Oudina F, Rashad AM, Ali HM, Sahnoun M, Ganaoui ME. Magnetohydrodynamic natural convection of hybrid nanofluid in a porous enclosure: numerical analysis of the entropy generation. *J Therm Anal Calorim.* 2020. <https://doi.org/10.1007/s10973-020-09690-z>.
 57. Babazadeh H, Shah Z, Ullah I, Kumam P, Shafee A. Analysis of hybrid nanofluid behavior within a porous cavity including Lorentz forces and radiation impacts. *J Therm Anal Calorim.* 2020. <https://doi.org/10.1007/s10973-020-09416-1>.
 58. Manh TD, Nam ND, Abdulrahman GK, Moradi R, Babazadeh H. Impact of MHD on hybrid nanomaterial free convective flow within a permeable region. *J Therm Anal Calorim.* 2020;140:2865–73.
 59. Biswas N, Manna NK. Enhanced convective heat transfer in lid-driven porous cavity with aspiration. *Int J Heat Mass Transf.* 2019;114:430–52.
 60. Biswas N, Manna NK, Datta P, Mahapatra PS. Analysis of heat transfer and pumping power for bottom-heated porous cavity saturated with Cu-water nanofluid. *Powder Technol.* 2018;326:356–69.
 61. Brinkman H. The viscosity of concentrated suspensions and solutions. *J Chem Phys.* 1952;20(4):571.
 62. Incropera FP, DeWitt DP. *Introduction to heat transfer.* New York: Wiley; 2002.
 63. Maxwell JC. *A treatise on electricity and magnetism.* Oxford: Clarendon Press; 1881.
 64. Suresh S, Venkataraj K, Selvakumar P, Chandrasekar M. Synthesis of Al₂O₃–Cu/water hybrid nanofluids using two step method and its thermo physical properties. *Colloids Surf A.* 2011;388(1–3):41–8.
 65. Patankar SV. *Numerical heat transfer and fluid flow.* New York: Hemisphere; 1980.
 66. Ghasemi B, Aminossadati SM, Raisi A. Magnetic field effect on natural convection in a nanofluid-filled square enclosure. *Int J Therm Sci.* 2011;50:1748–56.

Affiliations

Nirmalendu Biswas¹  · Nirmal K. Manna²  · Ali J. Chamkha^{3,4} 

✉ Ali J. Chamkha
alichamkha@duytan.edu.vn

Nirmalendu Biswas
nirmalendubiswas@yahoo.co.in

Nirmal K. Manna
nirmalkmannaju@gmail.com

² Department of Mechanical Engineering, Jadavpur University,
Kolkata 700032, India

³ Institute of Research and Development, Duy Tan University,
Da Nang 550000, Vietnam

⁴ Institute of Theoretical and Applied Research (ITAR), Duy
Tan University, Hanoi 100000, Vietnam

¹ Department of Power Engineering, Jadavpur University,
Salt Lake, Kolkata 700106, India